University of Massachusetts Lowell

Project: Peregrine Explorer

220 Pawtucket St, Suite #220

Lowell, MA 01851

NASA USLI Preliminary Design Review

October 28th, 2024

Table of Contents

Table of Figures

Acronyms

AGL = Above Ground Level

ACS = Altitude Control System

APCP = Ammonium Perchlorate Composite Propellant

ARCS = Avionics & Recovery Control System

CDR = Critical Design Review

CFR = Code of Federal Regulations

CG = Center of Gravity

CMASS = Central Massachusetts Spacemodeling Society

COTS = Commercial Off the Shelf

CP = Center of Pressure

DDIR = Dual Dissimilar Independent Redundancy

DOT = Department of Transportation

FAA = Federal Aviation Administration

FFF = Fused Filament Fabrication

FMEA = Failure Modes and Analysis

FN = Foreign National

FOV = Field of View

FS = Fully Successful

FRR = Flight Readiness Review

GPS = Global Positioning System

HPR = High Power Rocket

LCO = Launch Control Officer

LMS = Lawrence Lin Makerspace

LRR = Launch Readiness Review

MSDS = Material Safety Data Sheet

MSFC = Marshall Space Flight Center

MSL = Mean Sea Level

NAR = National Association of Rocketry

NFPA = National Fire Prevention Agency

PDF = Portable Document Format

PDR = Preliminary Design Review

PERR -C = Passive Electronic Recovery Reporter Capsule

PLAR = Post Launch Assessment Review

PPE = Personal Protective Equipment

RF = Radio Frequency

RFP = Request for Proposal

RSO = Range Safety Officer

SL = Student Launch

SLA = Stereolithography

SME = Subject Matter Expert

SOW = Statement of Work

STEM = Science Technology Engineering & Math

TRA = Tripoli Rocket Association

UML = University of Massachusetts Lowell

UMLRC = University of Massachusetts Lowell Rocketry Club

USLI = University Student Launch Initiative

VDF = Vehicle Demonstration Flight

1 Summary

University of Massachusetts Lowell Rocketry
Mailing Address: 220 Pawtucket Street, Suite #220. Lowell, MA. 01854 ATTN: UML Rocketry Club

Mentor: Howard Greenblatt, NAR#: 84058 Level 2 Certification
Email: h.greenblatt@comcast.net Phone: 617-797-1426

Final Launch Date: May 4th. Huntsville, Alabama.
Hours Spent on PDR: 560

Social Media Site	Handle
Instagram	@RiverhawkRocketry
Twitter / X	@rhrocketry
YouTube	@UMLRocketry
Website	Umlrocketry.org

1.1 "*Peregrine Explorer*" Vehicle Summary

Target Altitude	5500ft AGL
Motor Selection	Cesaroni Pro54-5G, K780 Blue Streak. Aerotech RMS 54/2560 K1275 Redline (Backup)
Outer Diameter	4.02in (10.2cm)
Independent Sections and masses	3 (Nosecone 2.65lbs, Upper Section 4.36lbs, Lower Section 5.90lbs)
Predicted Launch Mass	Primary: 16.7lbs (7556g). Backup: 17.4lbs (7890g).
Total Length	81.5in
Recovery System Style and Computers	Dual-Sep, Dual-Deploy. Telemetrum and Blue Raven
Parachute Sizing	Pilot / Nosecone: 24in. Main: 72in. Drogue: 18in.

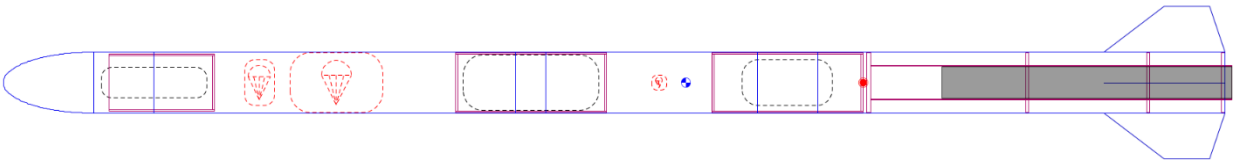

Figure 1.1.1: Open Rocket Diagram of Peregrine Explorer at the PDR Milestone

1.2 Payload Summary

UMLRC's 2024-2025 Payload experiment is divided into two systems, the Passive Electronic Recovery Reporting – Capsule (PERR-C) and the Altitude Control System (ACS). The nosecone of the vehicle will serve as the capsule's primary structural element. The system comprises of a custom sensor package and computer system PERR-C, fitted within the nosecone below the STEMNauts flight deck. Upon landing, the PERR-C system will transmit the data gathered by the custom sensor package via 2-M Radio back to NASA at the flight line. The ACS will assist the vehicle in hitting our target altitude.

2 Changes made since Proposal

2.1 Vehicle Design Modifications

We have made refinements to the Motor and Fin Assembly to make manufacturing the system easier. The recovery system remains largely unchanged from the proposal.

2.2 Payload Design Modifications

2.2.1 Primary Payload

The changes to PERR-C include adding a 2nd radio on the 900mhz band to facilitate communication to the primary payload to send commands to stop transmissions.

2.2.2 Secondary Payload

The changes to ACS include design modifications to improve payload function and the removal of the 900mhz radio transceiver that was moved to PERR-C.

2.3 Project Plan Modifications

2.3.1 Project Timeline

Since the proposal, minimal changes have been made to the project timeline. Work on the CDR was moved to start earlier than planned. Final vehicle design was shortened to ensure vehicle construction was completed by the end of December and testing was completed in early January. This was done to ensure that there would be sufficient opportunities to perform a test flight before March.

2.3.2 Team Member Updates

Since the proposal, we have welcomed Five new members onto the team. Three new Electrical and Computer Engineering Capstone Students, a 2nd-year Mechanical engineer to be the Assistant Safety Officer, and a new member to the Avionics and Recovery Team.

3 Vehicle Design

3.1 Vehicle Criteria

3.1.1 Mission Statement

Our team's mission is to create a modular high-powered rocket system and payload to reach 5500 ft AGL. The payload is an autonomous data reporter that will report data from on-board sensors recording information about Ascent, Descent, Landing, and the Landing zone. The team will use engineering skills learned in the classroom and will continue to educate members through valuable hands-on experience working with an engineering team.

3.1.2 Mission Success Criteria

1. Safely launch and recover the Launch Vehicle and payload
    a. Maintain stability throughout Ascent
    b. Recovery devices will deploy and work as intended
    c. All sections of the vehicle will be retained or descend in a safe and intended manner
2. The payloads will work as intended
    a. The primary Payload, PERR-C, will record data and report back to NASA's flight line via 2m radio.
        i. Full Success for PERR-C would be recording and transmitting all 8 data values to NASA clearly over 2m radio and ceasing transmission automatically without incident.
    b. The ACS will actively control the apogee of the vehicle to reach our target altitude.
        i. ACS Full Success would be attaining an altitude within 100 feet of the Target Altitude.
3. The vehicle will adhere to standard engineering and quality control practices during all phases of the project.
4. Make it to Huntsville, Alabama and launch on May 3rd and 4th.

- I don't know if you need it in paragraph form.

3.2 Vehicle Design Alternatives

3.2.1 Design Option 1

Our First Alternate design was a 6in Diameter Airframe, measuring 136in long. It would weigh 39lbs on the pad and would fly an L1395. This vehicle was designed to deploy the payload out of the vehicle's middle bay. The Nosecone is a 5:1 LV - Haack, it was selected because of the high aerodynamic performance throughout all flight regimes. Eventually, this design was disqualified because we did not need payload deployment to complete the Mission.

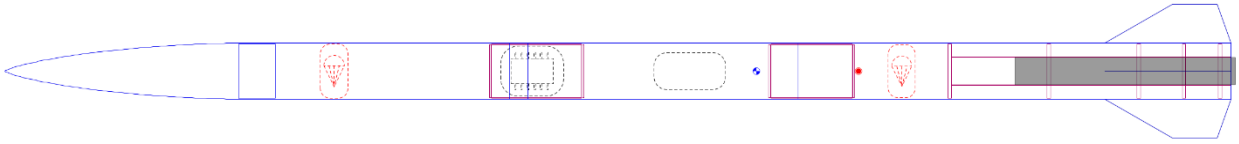

Figure 3.2.1: Alternate Vehicle Design 1 "CRX-251: 6in payload deploying Vehicle"

3.2.2 Design Option 2

Our 2nd alternative design was developed in parallel with our final design. It was designed to carry out the same flight profile and mission, on a larger 5.5 in airframe. This design would be 95in long, weighing 28.2lbs on the pad.

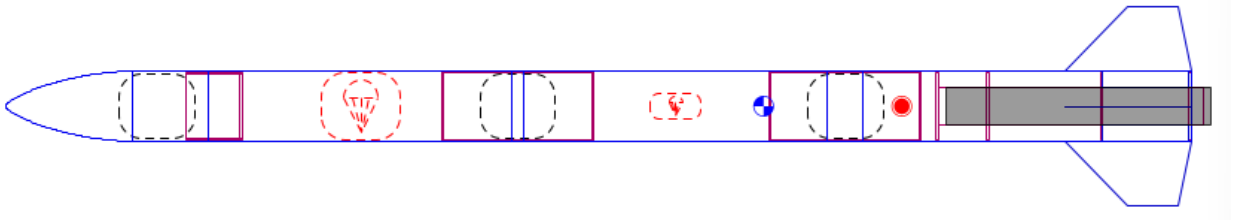

Figure 3.2.2: Alternate Vehicle Design 2 "CRX-252B: 5.5in Payload in Nosecone"

3.3 Final Vehicle Design

3.3.1 Design Overview

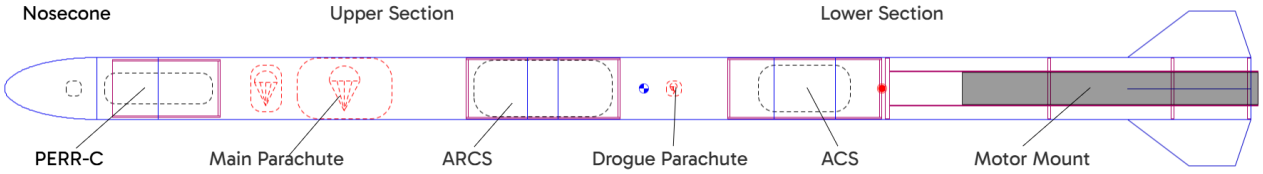

Figure 3.3.1: Vehicle Component Diagram

Peregrine Explorer is a modular, high-performance vehicle targeting a 5500-foot altitude and using the Cesaroni Pro54-5G K780 Blue Streak motor, with an Aerotech RMS 54/2560 K1275 Redline as a backup. With a 4.02-inch diameter and total length of 81.5 inches, the rocket's modular design supports quick assembly and optimal aerodynamics for achieving competitive performance. The primary payload includes two core systems: the Passive Electronic Recovery Reporting – Capsule (PERR-C) and the Altitude Control System (ACS). The nosecone doubles as the capsule's structural element and houses the custom PERR-C sensor package, which relays

data post-landing to NASA. The ACS enhances altitude control with an airbrake system to assist in precision flight to the target altitude.

The fin attachment offers two modular designs: a keyway with a locking cap and a bolt-through method. The first design locks the fins into place on the rail bracket with pins and a retaining cap, while the bolt-through method sandwiches the fins between the body tube and rail, providing additional rigidity and minimizing movement. The motor mount tube features “U” channels for fin attachment, while centering rings and the inner tube are fixed with epoxy for added durability. The rocket's modular fins, available in several profiles, contribute to stability and aerodynamic performance, with an airfoil profile ultimately chosen for their efficiency in reaching higher altitudes at optimal velocities.

The avionics and recovery systems, housed within the ARCS, utilize redundant Telemetrum V4 and Blue Raven computers, ensuring reliable data collection and safe descent. ARCS incorporates a unique triangular sled configuration for secure and independent functionality of each system. The ARCS module provides full telemetry via HAM radio, and the onboard systems are accessible for adjustments through an external control panel. This configuration includes multiple safeguards, such as a physical arming pin and USB-C connectors for quick access to power and data, facilitating thorough monitoring and seamless recovery.

Supporting the payload mission, PERR-C communicates key flight metrics to ground stations via a 915 MHz ground station and a 144 MHz radio. Meanwhile, the ACS employs a dedicated guidance system that activates post-motor burnout, adjusting airbrake deflection to maintain the targeted altitude. Constructed using PLA and PETG, the PERR-C nosecone design integrates a durable structure for holding sensor packages while allowing visibility and easy internal access. Together, these innovations enable the *Peregrine Explorer* to meet stringent recovery and altitude accuracy criteria in alignment with NASA’s scoring metrics.

3.3.2 Motor and Fin Assembly

3.3.2.1 Design Rationale

The fin and rail bracket assembly are designed to keep the rocket stable, adaptable, and efficient during flight. The rail bracket is modular, making it secure and easy to adjust, while different fin options help improve flight performance. This setup supports stable, low-drag, and high-altitude flights to meet the different mission needs

3.3.2.2 Overall Design

The design features a modular fin and rail bracket assembly made for stability and aerodynamic efficiency. The primary subassembly, the rail bracket, is a cylindrical piece with four channels allowing for precise rail mounting, which is glued to the motor tube. The fin section supports interchangeable fin profiles for improved aerodynamic performance. The final design aims for even distribution of aerodynamic forces, contributing to stable flight.

3.3.2.2.1 Alternate Designs

In the rail bracket design, a bolt-through alternative allows for a modular setup where fins and components can be easily adjusted or replaced. This approach includes a flange extending into the thruster body by 1.5 inches, with two holes drilled for inserting pegs, enabling secure positioning within the thruster body. Alternatively, the holes can be left open to accommodate bolts, creating a "sandwich" mount that compresses the fin and bracket assembly together. This flexibility in mounting provides options to fine-tune the connection's stability and strength, supporting the design's adaptability to different mission or load requirements.

Alternate fin designs focus on aerodynamic performance and stability. Clipped delta fins, known for their truncated shape, minimize drag while enhancing lift, making them ideal for reaching higher altitudes. Swept fins are also viable, as their backward-angled shape reduces drag at high velocities, promoting smooth airflow and efficient flight. Elliptical fins offer an option geared toward achieving maximum altitude; their shape efficiently distributes aerodynamic forces, further minimizing drag while maintaining a low profile. These alternative profiles provide options for tailoring the rocket’s performance to specific flight goals

3.3.2.3 Subassemblies and Components

The first subassembly is the rail bracket connecting to each rail. The rail bracket is a cylinder with 4 channels cut into it to allow for the mounting of the rails. The rails will be glued to the rail bracket with is glued to the motor tube. The rail brackets might change depending on bolt or sliding fit design choice. The fins on the sliding bolt design will have a normal fin with a flange sticking into the thruster body 1.5 inches. On this flange 2 holes will be drilled where 2 pegs are inserted. A second alternative is leaving the holes drilled so a bolt can be threaded through to do the sandwich design.

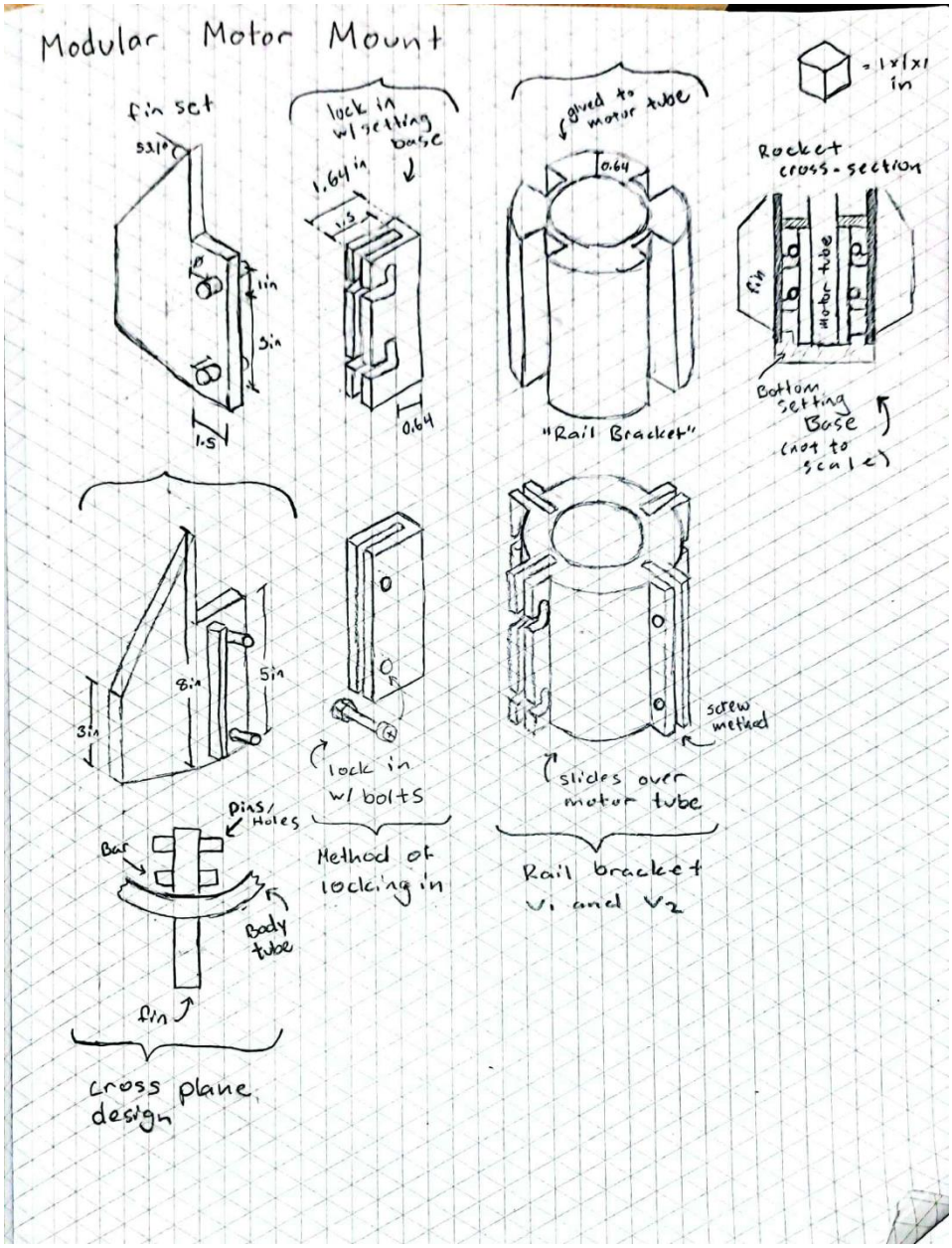

Figure 3.3.x: Interchangeable Fin Section Concept Drawing

3.3.3 Fin Design

Fin designs include rectangular, rounded, and aero foil profiles. The purpose of a rectangular profile is that the fins are simpler and cheaper to manufacture and can be made as one part. They do not perform as well aerodynamically as the rounded or aero foil profiles. The rounded should perform slightly better than the rectangular, while manufacturing with a similar ease and process. The aero foil design is ultimately the most efficient and aerodynamic but is the most complex and expensive. It cannot be manufactured as one piece with the available supplies. This would result in it being made of several spars and laid over with a skin of a different material, or 3D printed as a shell. The chosen aero foil fin design is modeled with measurements of 8 inches for the root chord length, 3 inches for the tip chord length, 3 inches for the height, and 4 inches for the sweep length creating a sweep angle of 53.1 degrees.

Feasible alternative fin design options include clipped delta fins, swept fins, elliptical fins, etc. Clipped delta fins and swept fins would be more suitable options for trying to achieve higher altitudes at greater velocities. Elliptical fins are also designed for maximum altitude at a high performance while generating a low amount of drag.

Our final design has fins evenly distributing aerodynamic forces to help with stability during flight.

Criteria	Rectangular Profile	Rounded Profile	Aerofoil Profile
Aerodynamic Performance	1 (Lowest)	2 (Moderate)	3 (Highest)
Manufacturing Simplicity	3 (Simplest)	2 (Moderate)	1 (Most Complex)
Cost	3 (Lowest)	2 (Moderate)	1 (Highest)
Material Complexity	3 (One-piece design)	3 (One-piece design)	1 (Multi-part/shell)

Table 3.3.1: Comparison Matrix of Different Fin Profile Designs

3.3.5 Nosecone / PERR - C

The nosecone is a 1.5:1 elliptical nosecone, and it is designed to house the Primary Payload. The Nosecone section is made of 3 main parts, the Elliptical nosecone, a small cylindrical extension to add more volume, and the shoulder to attach the nosecone to the rest of the vehicle. The considerations into the design of the nosecone are discussed in 4.2 Passive Electronic Recovery Reporter – Capsule.

3.4 Avionics and Recovery System

3.4.1 Avionics and Recovery Criteria

3.4.1.1 Mission Statement

The Avionics and Recovery Control System (ARCS) is designed with simplicity at the forefront. Redundancy is integrated into all aspects, ranging from flight computer selection to the physical location of components inside the bay. Redundancy exists across data collection methods, and both physical and software redundancy exists for parachute deployment and timing. Parachute selection is optimal for scoring, while providing the vehicle and tethered components with a safe descent regardless of the circumstance. The main mission is to return the vehicle to the ground in the highest-scoring mode possible, while allowing the payload the opportunity to safely deploy and conduct its science objectives.

3.4.1.2 Mission Success Criteria

Mission success criteria have been established for ARCS performance in flight. ARCS primary success criteria include returning the vehicle to the ground safely, landing with no unfired ejection charges, and demonstrating successful ejection of parachutes on primary ejection. These criteria are considered a Full Success (FS) if: the vehicle descends from apogee at its nominal decent rate (as simulated) and subsequently descends under the main parachute at its nominal decent rate (as simulated), all ejection charges fire on-time (as validated using service cameras and on-board audio), and both parachutes are ejected and deployed by the primary ejection charge (redundancy is not used).

3.4.2 System Overview

ARCS is a 500-gram avionics and recovery system that utilizes an Altus Metrum Telemetrum V4 as the primary flight computer, and a Featherweight Altimeters Blue Raven as the redundant/secondary flight computer. These systems operate on completely separate peripherals (battery, arming hardware, mounting hardware, and vehicle location), and offer redundant data capabilities when packaged together. Telemetrum V4 can transmit live telemetry over HAM radio frequency, allowing telemetry of the flight to be analyzed when visual of the vehicle is lost, in real time. Blue Raven has an impressive suite of sensors and software redundancy, that offers a 3-axis gyroscope and tilt sensor, while maintaining redundancy across all critical flight data from the primary flight computer (barometric altitude, accelerometer, battery voltages, ejection timings, etc.).

ARCS is internally divided into three sleds oriented in a triangular configuration. Each sled will operate independently of the rest, but all sleds will exist in an enclosed, shared space where pressure can equalize between all the computers. The interior of the triangular section is used to route ejection charge wiring, camera systems, and all potential electromagnetic generating wiring arrangements, as it will be insulated with aluminum sheeting and aluminum tape. All computers and utilities will be fully accessible from the exterior of the bay via a door mounted on the switch-band.

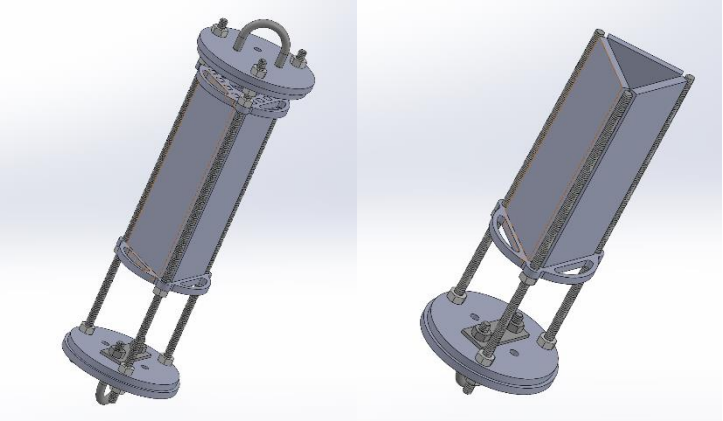

Figure 3.4.2: Basic triangular structure of ARCS bay (Left: Full structure, Right: Cross-section to show inner triangle).

The interior triangular sled configuration is divided into Sled A, Sled B, and Sled C, as follows:

- **Sled A:** Sled A, also called the Primary Avionics Sled (Section 3.4.3.5), will have the main flight computer, Altus Metrum Telemetrum V4 and its battery.
- **Sled B:** Sled B, also called the Secondary Avionics Sled (Section 3.4.3.6), will have the redundant flight computer, Featherweight Altimeters' Blue Raven and its battery.
- **Sled C:** Sled C, also called the Service Camera Sled (Section 3.4.3.7), will harbor the two computers for our exterior cameras as well as their batteries.

The space above the triangular sled structure will be modular, offering room for additional modules such as ballast, battery storage, or a secondary antenna.

All the onboard systems will be accessible behind an exterior panel attached to the coupler tube using a machine screw and 3D-printed hardware. Under the panel will be a small junction box, allowing access to 2 USB-C connectors for battery charging and data offload, as well as 3 screw switches for arming the flight computers on the pad. Also, the system will offer further ordinance redundancy in the form of a physical, threaded shoulder bolt arming pin.

3.4.3 Components and Alternatives

3.4.3.1 Coupler and Switch Band

The avionics will be housed within a 10-inch tall, 3.6-inch inner diameter fiberglass tube from Wildman Rocketry. These materials were selected as the primary fuselage material.

The fore shoulder of the avionics coupler is classified as not-in-flight and is secured 3-inches (0.75x of vehicle's outer diameter) into the rocket's fuselage with 6 evenly spaced, radial 4-40 machine screws.

The top of the switch band is located below the 3-inch not-in-flight shoulder on the fore of the coupler. It is 3-inches in length and will match the 4-inch outer diameter of the vehicle, with a tight tolerance with the 3.8-inch diameter coupler tube. The switch band will be secured in position using epoxy.

The aft shoulder of the avionics bay is classified as in-flight and is 4-inches in length (1.0x the vehicle's outer diameter). The aft shoulder will utilize a configuration of evenly spaced shear pins to secure itself into the respective fuselage.

3.4.3.2 Primary and Redundant Altimeters

The Altus Metrum Telemetrum V4 was chosen as the primary flight computer, and the Featherweight Altimeters Blue Raven operates as the redundant/secondary flight computer. Multiple reasons lead to this computer arrangement being chosen. The most important consideration is that both flight computers have had successful flights on various past team vehicles. This indicates the reliability of each computer and therefore they are deemed trustworthy. It is critical to run two different computers/systems for redundancy, but in this case, it also gives the avionics further functionality when the two are run in unison. Blue Raven has integrated software and data redundancies while Telemetrum brings live telemetry capabilities through HAM radio. The availability of these two computer systems was also an important factor. Additionally, considerable financial investment in these two computers was made in the past, and therefore continued use is a very cost-effective practice, further justifying the decision to use them.

3.4.3.3 Ejection Charges

Having properly functioning ejection charges is the defining factor in a successful, and more importantly, safe flight. This leads to the necessity to have a high quantity of backups and redundancies to ensure a safe flight at any cost. Both main and drogue parachutes have primary and secondary/redundant ejection charges to fill this need. The redundant charges have a huge reliance to properly function if the primary were to fail. Because of this, a 1.25x multiplier on the required force of the charge is put onto the calculations for redundant charge mass. This is in place to ensure the separation of the vehicle along with proper parachute deployment in all potential cases. The physical sizes of these charges are related to one another: The main parachute primary charge is the smallest of the charges, the main parachute redundant and drogue primary charges will be roughly the same size, and the largest charge will be the drogue redundant charge.

These charges allow for variable pressures scaling with both the volume being expanded, the structural limitations of the fuselage, and the relative risk associated with dynamic conditions at time of detonation.

For example, it is critical that the drogue charges detonate and eject the parachute. At apogee (when the drogue charges detonate) the charge must overpower the drag force on the nosecone, decrease the inertia of the vehicle, and must be powerful enough to break the shear pins. Therefore, the drogue primary charge is sized for a perfect scenario, and the drogue redundant charge is sized larger than the primary, in case of an off-nominal scenario, to maintain redundancy of deployment. The main parachute charges are smaller than the drogue charges, because they have less forces acting to oppose them as they fall under the drogue parachute. The relationship between the main primary and main redundant charge sizes aligns with that of the drogue charges (redundant charge is greater in size than primary to account for off-nominal deployment conditions).

Additionally, a gas piston will be used to apply equal pressure among all internal parachutes and cords. This piston will utilize a heat-shielded bulkhead attached to a length of internal coupler tubing (tolerance of +0”/-0.002” in diameter to the ID of main body tubing) to create an airtight volume above the ejection charges. This piston is

tethered using several knots and through holes, allowing for the piston to remain tethered to the shock cord once it reaches the end of the body fuselage. The piston will exist in the main parachute bay only, and its purpose is to enhance the ejection charges' ability to push on the parachutes and recovery hardware and eliminate any chance of gas leakage past the main recovery hardware. The drogue ejection charge positioning does not allow for a gas piston to exist to deploy the drogue parachute, so traditional means of ejecting the drogues will be used instead.

Finally, a physical arming pin will use vibration resistant limit switches to physically disconnect the ejection charges from the flight computers until after the computers are armed on the launch rail at the pad.

$$Grams(BP) = \frac{454grams}{1lbf} \times \frac{Pressure(psi) \times Volume(inches^3)}{266\frac{inches \bullet lbf}{lbm} \times 3307 \circ R}$$

Figure 3.4.3.3: Formula used to calculate ejection charge (black powder) masses.

The black powder mass of all ejection charges was calculated as follows:

- **Main Primary:** 1.55 grams (produces 15.4 psi)
- **Main Redundant:** 1.95 grams (produces 20 psi)
- **Drogue Primary:** 0.68 grams (produces 15.4 psi)
- **Drogue Redundant:** 0.85 grams (produces 20 psi)

3.4.3.4 Switches & Switch Holder

The switches and switch holder provide access to an internal panel, allowing for the arming and initiating of the flight computers, batteries, and ejection charges through individual screw switches. In addition, USB-C ports are included to connect both flight computers individually, allowing for data offloading and battery charging with a single cable. The switch door is attached using a single Phillips head 4-40 machine screw to a 3D-printed offset mounted over the secondary/redundant flight computer sled. This design offers sufficient clearance with the coupler tube, making disassembly of the bay simpler while avoiding interference between the wiring and coupler tube itself. If the switches were directly attached to the coupler, they would interfere with internal components, so this design was chosen to avoid that issue.

Additionally, a small oval cutout in the switch band allows for two on-board cameras to be housed internally. This cutout would be covered with a thin piece of plastic film, and the cameras would be mounted closely to the internal surface of the coupler tube. More information about this configuration is outlined in Section 3.4.3.7.

In short, the setup is a 3D-printed junction box style container mounted on the secondary avionics sled, housing the screw switches and USB-C ports. This box is accessible through a

hole in the coupler tube's switch band, covered by a removable door attached with a 4-40 machine screw. This box is precisely aligned with the bay's internals using clocking marks on the bulkheads and coupler tube for alignment before integration.

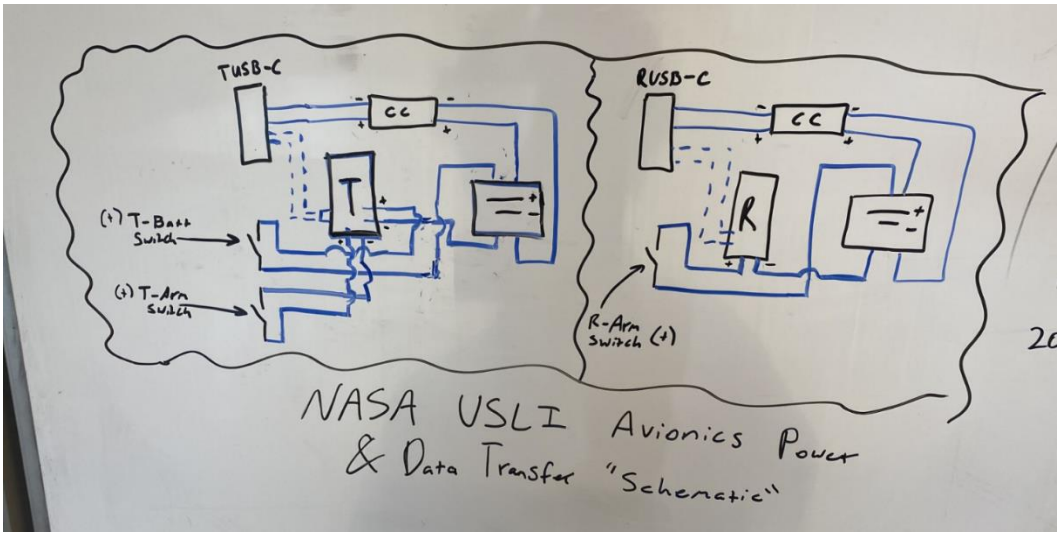

Figure 3.4.1: Data Transfer and Battery Charging electrical schematic (sketch).

The overall design of the avionics bay ensures that the batteries and flight computer data are easily accessible without having to disassemble the bay completely between flights. This allows for easy data access and battery maintenance without removing bulkheads or disconnecting the coupler tube.

3.4.3.5 Primary Avionics Sled

The Primary Avionics Sled houses the primary flight computer (Telemetrum V4) along with its battery and wiring. To maximize space, the altimeter is mounted vertically at the top of the sled to allow for its 6-inch integrated antenna to extend downwards uninhibited. The battery is mounted adjacent to the flight computer, on the same side of the bay. The main feature of this layout is maintaining a straight, uninhibited line along the sled surface so the antenna on the primary flight computer can operate at its full capability, maximizing radio range.

An alternative design included mounting the battery on the opposite side of the primary avionics sled. This configuration would make accessing the batteries difficult if they needed to be serviced. Additionally, LiPo batteries are comprised of volatile components that can degrade/react over time, and so maintaining a visual on the battery while not in use is crucial to personal and system safety.

3.4.3.6 Secondary Avionics Sled

The Secondary Avionics Sled houses the secondary flight computer (Blue Raven) and all its peripherals (battery and wiring). The secondary flight computer's form factor is significantly smaller than the primary flight computer, and it does not include any sort of radio/antenna. This allows the secondary flight computer and its battery to fit comfortably on the top half of the avionics sled. The bottom half of the sled is dedicated to the junction box for the initiation switches and USB-C ports for charging and data offload, as outlined in Section 3.4.3.4.

Similarly to the primary avionics sled, the secondary avionics sled considered mounting its battery on the rear side of the sled, however this concept was eliminated because of the safety issues associated with not having a visual on the LiPo batteries.

3.4.3.7 Service Camera Sled

The Service Camera Sled houses two RunCam FPV drone cameras and their respective electrical components and hardware. On the sled, a 3D-printed structure will position the cameras (one facing aft, one facing fore) in position with the oval cutout in the coupler's switch band. This structure will be attached between the two square electronics packages (one for each camera) at the top end of the sled. The battery for the cameras is mounted longitudinally across the bottom of the sled. Adjacent to the battery, an arming circuit to initiate the cameras at moment of launch will be mounted. All wiring for the cameras will reside in the EMI shielded region behind all the sleds in the bay.

3.4.3.8 Batteries and Battery Guards

For power, we selected 1S LiPo batteries due to their 4.2 V output, which matches the nominal voltage requirements for both altimeters, ensuring optimal performance. The batteries are sized at 450 mAh for Blue Raven (secondary/redundant flight computer) and 900 mAh for Telemetrum V4 (primary flight computer), to accommodate for the necessary pad time and data logging for the entire flight duration.

3.4.3.9 Attachment Hardware

The attachment hardware for the rocket includes many components to secure multiple parts for safe flight. Size 4-40 pan-head bolts are used to attach the electronics to their respective sleds, while providing a low-profile head that will distribute force evenly on the components. These are paired with 4-40 square nuts to provide stability and reduce the risk of loosening in flight. These square nuts can be easily integrated into 3D-printed and laser-cut structural components. The number and radial spacing of the shear pins are chosen strategically based on the size of parachute ejection charge to control the separation of sections during deployment events. Shear pins are designed to hold during ascent and only break under a specific load, giving us more control over the deployment timing of the rocket. Standard nuts and lock nuts are also used to add an extra layer of security on the frame of the bay, with lock nuts preventing loosening from vibrations during flight.

3.4.3.10 Tracking Devices

The only tracking device on ARCS is the GPS and position data integrated into the primary flight computer (Telemetrum V4). The battery for this computer is 900 mAh to provide more than 30 minutes of GPS and telemetry pings after landing to locate the vehicle's position.

3.4.4 Parachute Sizing

A 72-inch main parachute and a 12-inch drogue parachute configuration allows the vehicle to have a controlled descent in just above 80 seconds, which is optimal for scoring.

Additionally, a reefing ring will be used to limit the inflation of the main parachute, reducing the shock felt by the vehicle as it inflates. The drogue parachute diameter was chosen to maximize a safe, controlled decent velocity, and minimize drift from the wind. Additional parachute/recovery information is outlined in Section 3.4.5.

3.4.5 Current Recovery Design

The configuration that has been determined to perform the best within the desired flight envelope includes a combination of parachute sizing, shock cord lengths, shock chord diameter and material, anchor point hardware and location, and the strength ratings of these components.

The current parachute sizing includes:

- **12-inch diameter drogue parachute:** 147 ft/s nominal decent rate, deployed at apogee, allows rapid, controlled decent with minimal wind response/drift.
- **72-inch diameter main parachute:** 13.25 ft/s nominal decent rate, deployed >500 ft AGL, decelerates vehicle slowly using a reefing ring to limit parachute inflation time. This parachute also grants the lowest kinetic energy at landing, ensuring all flight components remain intact and data can be extracted post-flight.

Alternatives that have been considered consist of an 18-inch drogue parachute paired with a 56-inch main parachute, and a 24-inch drogue paired with a 48-inch main parachute. However, the kinetic energy at landing and the wind drift experienced by these other configurations are unfavorable. These alternatives compromise the vehicle's capability to land and be recovered within the time limit and radius targeted to maximize scoring.

The current shock cord length varies between dictions of the vehicle. Based on analysis of parachute clearance, payload clearance, and landing/impact timing, the shock cord lengths from nose to fin can are as follows:

- **Cord A: Nosecone / PERR-C attached to ARCS**: This cord length is 30 feet. The payload descends under its own parachute, and so, to avoid entanglement with the main parachute, the length must be significant enough to physically separate PERR-C while remaining tethered.
- **Cord B: Main Parachute attached to ARCS:** This cord length is 15 feet. This length equally spaces the main parachute between the vehicle and PERR-C, minimizing risk of entanglement

- **Cord C: ARCS attached to ACS:** This cord length is 15 feet. This cord length grants ample separation between sections of the vehicle without inhibiting drogue parachute position. The drogue parachute will be attached on a bite knot 10 feet from the ARCS side of this length (located in the lower third of Cord C). This unequal positioning of the drogue parachute minimizes the chance of the fore fuselage colliding with the much higher drag aft (fin can and ACS) fuselage during decent.

The cord (diameter and material) selected for all shock cords is ½-inch diameter, Nylon strapping cord. This cord boasts high temperature resistance from hot gas, exceptional tensile strength for shock loading, and chemical resistance from exposure to corrosive environments. Kevlar was considered for this application because of its similar strength characteristics, but Nylon Strapping was ultimately selected.

The ½-inch diameter nylon strapping can support about 1,000 lb. tensile load and is rated for constant loading at 120 lb. This is ideal for both the shock loading and the fatigue loading that the shock cord will endure during flight.

All shock cords will be anchored firmly to a composite plywood bulkhead with a 304 stainless steel U-bolt. The U-bolt is secured to the bulkhead using washers and locknuts to mitigate loosening due to vibrations.

Based on prior flights with composite plywood bulkheads and steel hardware, the strength of the bulkheads is capable of withstanding violent parachute shock loads without cracking, delaminating, or dislodging attached hardware. Analysis of past flights suggests that these composite plywood bulkheads will handle a 1,200 lb. shock load with FOS greater than 2.0.

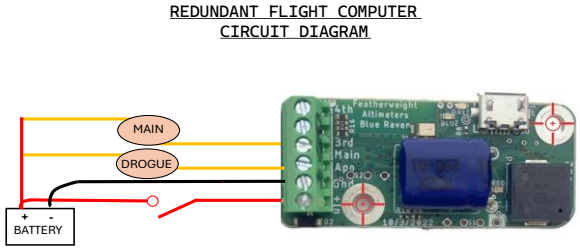

Figure 3.4.2: Blue Raven Circuit Diagram

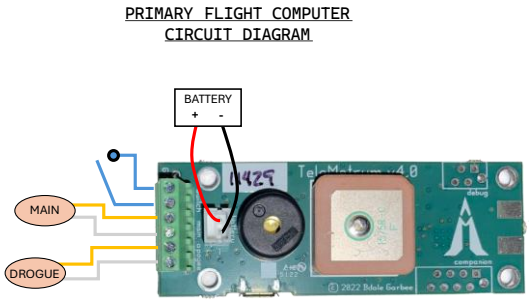

Figure 3.4.3: Telemetrum Circuit Diagram

3.4.6 On-Board Service Cameras

The On-Board Service Cameras will be attached to ARCS and will provide service footage of both the fore and aft of the ARCS bay. The fore camera will document the main parachute and payload parachute ejection events, and the aft camera will document the drogue ejection and parachute inflation events.

Multiple methods of activating the cameras have been discussed because of the long pad time specified in the launch rules/itinerary. The camera bay will utilize one of the two auxiliary outputs on the redundant/secondary flight computer to command the cameras to begin recording when the flight computer detects liftoff. The computers will then be powered on via a mosfet and a microprocessor. Additionally, the cameras will be powered using a 2S 750 mAh lipo battery. This power configuration provides approximately 1 hour of power for the cameras, at 2.6K resolution at 60 frames per second. At 1 hour long each video file will be approximately 3GB.

3.5 Mission Performance Predictions

3.5.1 Motor Selection

Manufacturer	Engine Selection	Engine code	Diameter (mm)	Length (mm)	Burn time (s)	Total Impulse (N-s)	Avg. Thrust (N)
Cesaroni	Primary	2114K780-15A	54	489	2.72	2114	778
Aerotech	Backup	2138K1275R - P	54	549.1	1.84	2138	1275

Table 3.5.1: Motor Specifications

3.3.1.1 Alternate Motors and Selection Rationale

Other motors were considered for the selection of our Primary and Backup Motors. Some of note were the Cesaroni Pro54-4G K740 C-Star, the Cesaroni Pro54-5G K635 Classic. These motors would fly within the mission required altitude, but lower than the selected motor. However, we ultimately chose the K780BS as our primary motor as the club has used the motor before, and we already own hardware for that motor.

We chose the Aerotech K1275 as it was the closest motor, performance-wise, to the CTI K780BS. We decided to go with Aerotech for our backup motor as CTI has been having issues stemming from a fire at their production facility in 2016 and has been affected by supply chain issues that have been happening across the globe. There have been sporadic updates from CTI retailers on “the Rocketry Forum” stating that CTI stock would ship “No Earlier Than October 2024”

3.5.2 Flight Profile Simulations

Flight simulations to calculate the flight profile were performed in OpenRocket and RASAero II. In OpenRocket and RASAero II, all flight simulations assumed a launch from sea level, and a 5-degree launch angle, the minimum launch angle set by NASA, as well as a wind speed of 0 MPH. The simulation gathered the data for the rocket's altitude, vertical velocity, and vertical acceleration for both the primary and backup motors.

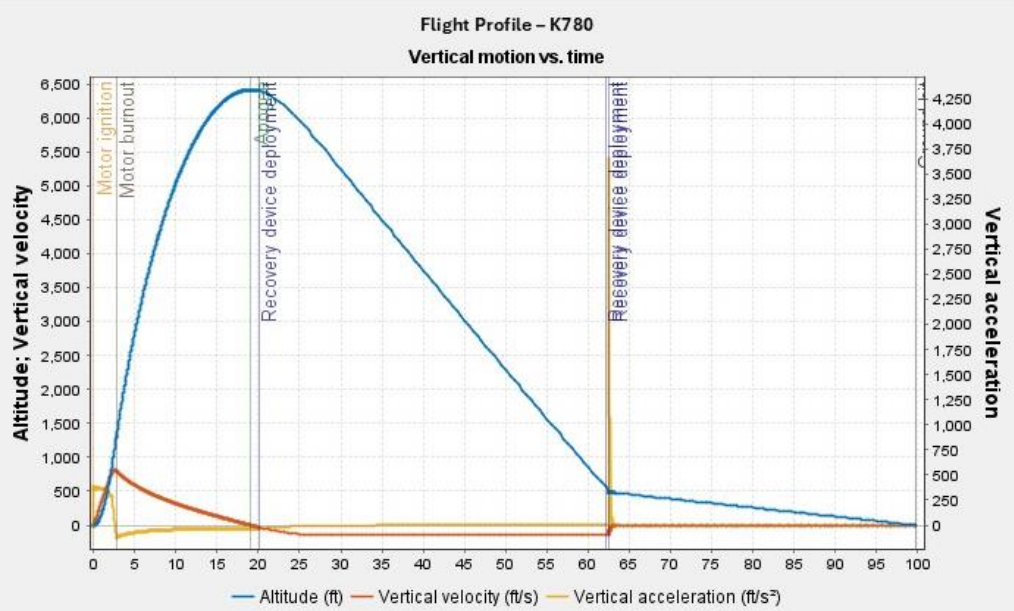

Figure 3.5.1: OpenRocket flight profile simulation for the Cesaroni K780 motor with altitude, vertical velocity, and vertical acceleration over time

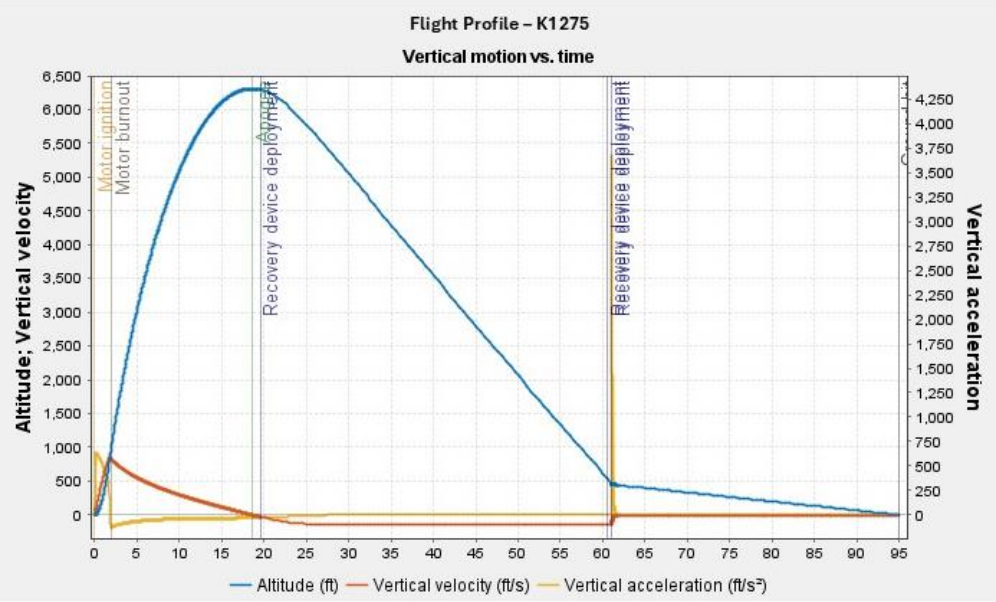

Figure 3.5.2: OpenRocket flight profile simulation for the Aerotech K1275 motor with altitude, vertical velocity, and vertical acceleration over time

Using the Ceseroni K780 motor in OpenRocket, the apogee was 6418 ft (1956 m), the maximum velocity was 816 ft/s (249 m/s), and the maximum acceleration was 390 ft/s^2 (119 m/s^2). For the backup motor, the Aerotech K1275, the apogee was 6306 ft (1922 m), the maximum velocity was 843 ft/s (257 m/s), and the maximum acceleration was 623 ft/s^2 (190 m/s^2). The two simulations calculate similar apogee and maximum velocity between the two motors. The main difference is the maximum acceleration, which shows the primary motor, the K780, having a lower maximum acceleration by about 46%.

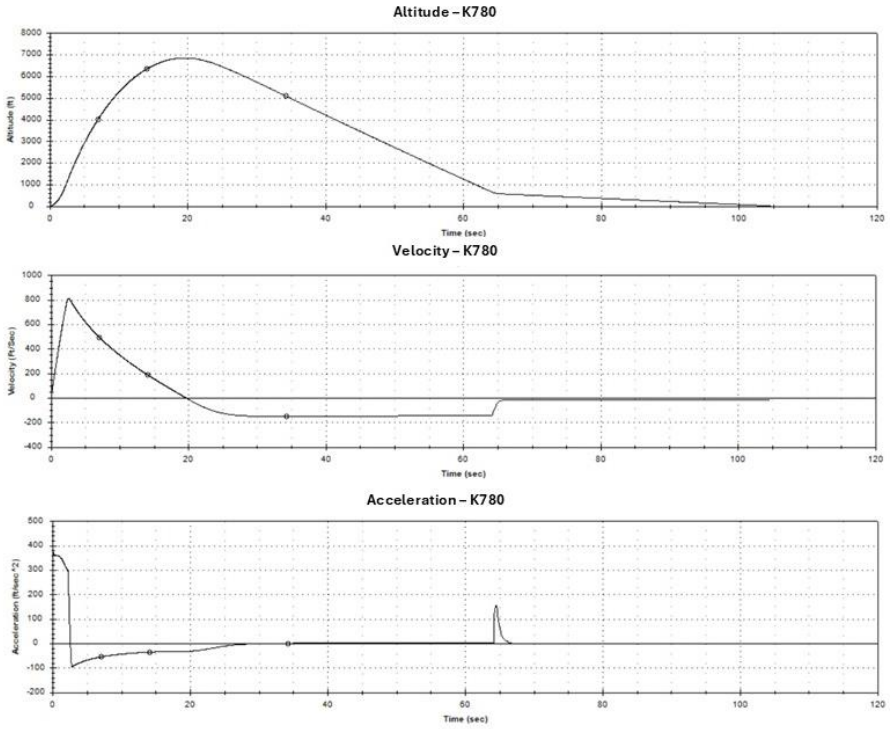

Figure 3.5.3: RASAero II flight profile simulation for the Cesaroni K780 motor with altitude, vertical velocity, and vertical acceleration over time

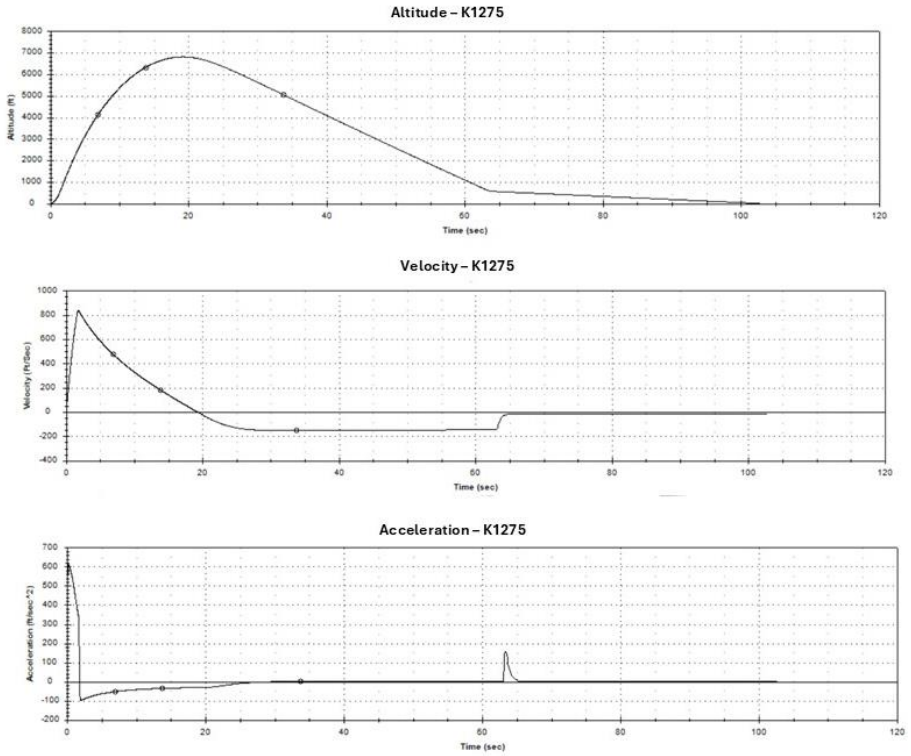

Figure 3.5.4: RASAero II flight profile simulation for the Aerotech K1275 motor with altitude, vertical velocity, and vertical acceleration over time

Using the Ceseroni K780 motor in RASAero II, the apogee was 6843 ft (2086 m), the maximum velocity was 834 ft/s (254 m/s), and the maximum acceleration was 400 ft/s^2 (122 m/s^2). For the backup motor, the Aerotech K1275, the apogee was 6805 ft (2074 m), the maximum velocity was 859 ft/s (262 m/s), and the maximum acceleration was 620 ft/s^2 (189 m/s^2). The two simulations calculate similar apogee and maximum velocity between the two motors. Similarly, the main difference is the maximum acceleration, which shows the primary motor, the K780, having a lower maximum acceleration by about 46%.

The RASAero II simulation data was observed to be consistently higher than the simulated data from OpenRocket. The difference is likely due to how OpenRocket handles transonic flight calculations, as well as differences in how each software is set up and how they calculate data.

3.5.3 Stability Margin

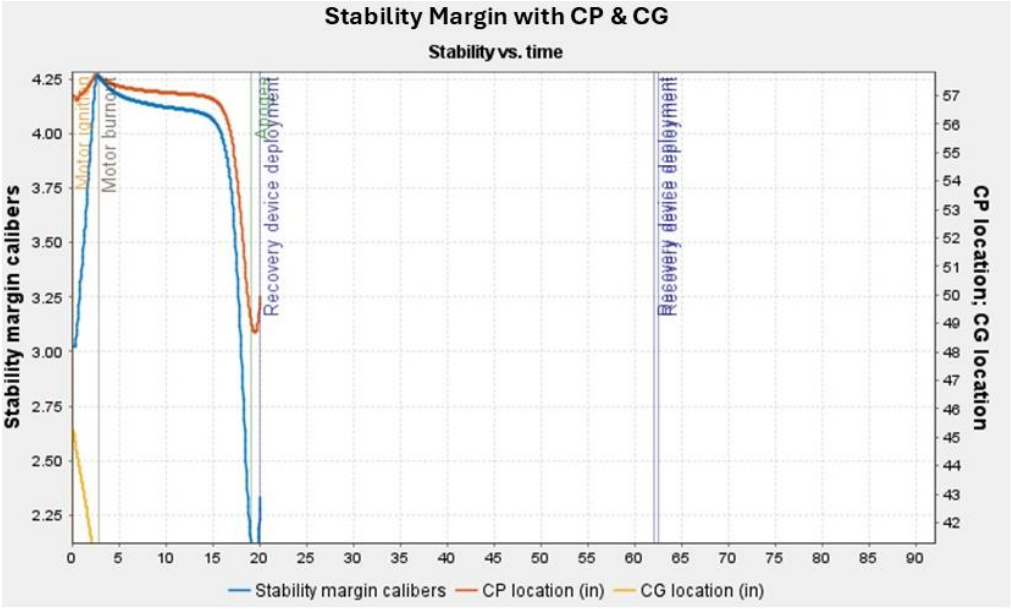

Figure 3.5.5: OpenRocket stability margin, center of pressure location, and center of gravity location over time

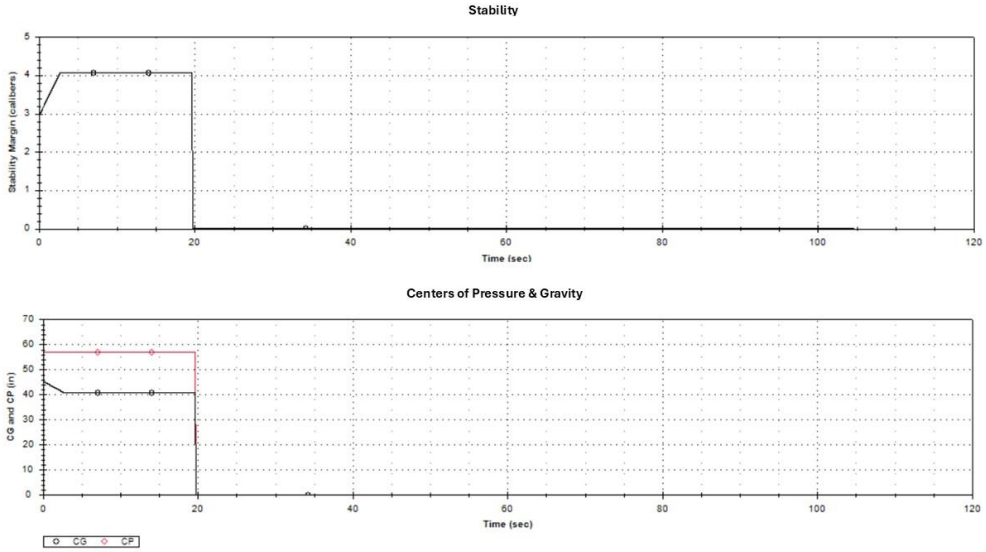

Figure 3.5.6: RASAero II stability margin, center of pressure location, and center of gravity location over time

On the pad with no ballast, the vehicle has a static stability of 2.93 calibers, and at rail exit (50.5ft) has a stability of 2.98 calibers. The center of gravity is located at 45.27in from the tip of the nosecone, which is in the middle of the drogue parachute bay. The center of pressure is located 57.03in from the tip of the nosecone, which is only ~3 aft of where the ACS will deploy from. Because of this, we believe that the ACS will pose little to no effect on the static stability of the vehicle.

3.5.4 Landing Calculations

3.5.4.1 Kinetic Energy at Landing

The worst-case scenario ground hit velocity is 12.86ft/s (3.92m/s) and is assumed for the following calculations. After all deployments, the launch vehicle will be in 3 sections; From fore to aft, the masses of each section, including parachutes, are: PERR-C is 2.653 lb, Upper-Section (Main Chute bay, ARCS) is 4.36 lb, Lower-Section (drogue chute bay, ACS, Motor Mount, Spent Motor) is 7.14 lb. This mass assumes the K780 motor, the Lower-Section's mass with a spent K1275 motor is 7.59lb. With the worst-case scenario ground hit velocity, at ground hit, these segments will have kinetic energies of 6.82 lbf*ft, 11.21 lbf*ft, and 18.35 lbf*ft (19.51 lbf*ft with the K1275 motor), respectively.

3.5.4.2 Descent Time

All components of the vehicle are tethered together, and therefore all have the same descent time. On the OpenRocket simulations, with no wind, apogee is reached at T+19 seconds, and the vehicle hits the ground at T+101 seconds, for a total descent time of 82 seconds. This is the simulation with the longest total flight time.

Under the drogue parachute (12-inch diameter) the decent rate is 147 ft/s (45 m/s), and under the main parachute (72-inch diameter) the decent rate is 13.25 ft/s (4.04 m/s) in the nominal case.

3.5.4.3 Drift Simulations

Drift simulations were completed with simulated wind speeds ranging from 0 to 20 miles per hour. Each simulation increased the wind speed by an increment of 5 mph. The drift simulations were completed using a 10-degree launch angle to account for the most extreme launch angle. The simulations also assumed the rocket was traveling against the wind.

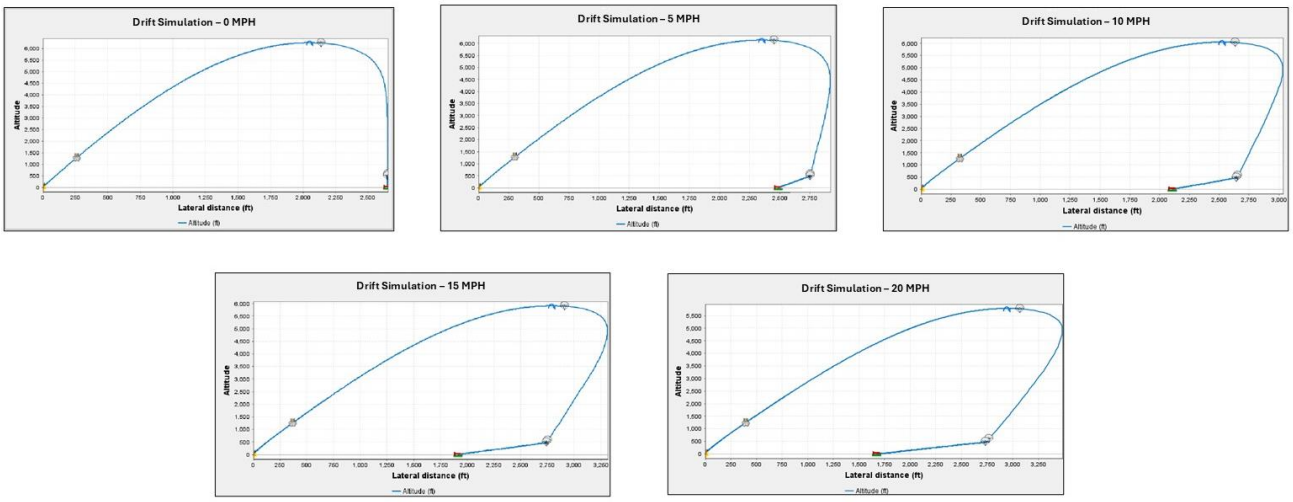

Figure 3.5.7: OpenRocket altitude over lateral distance simulations at winds speeds from 0-20 MPH by increments of 5 MPH

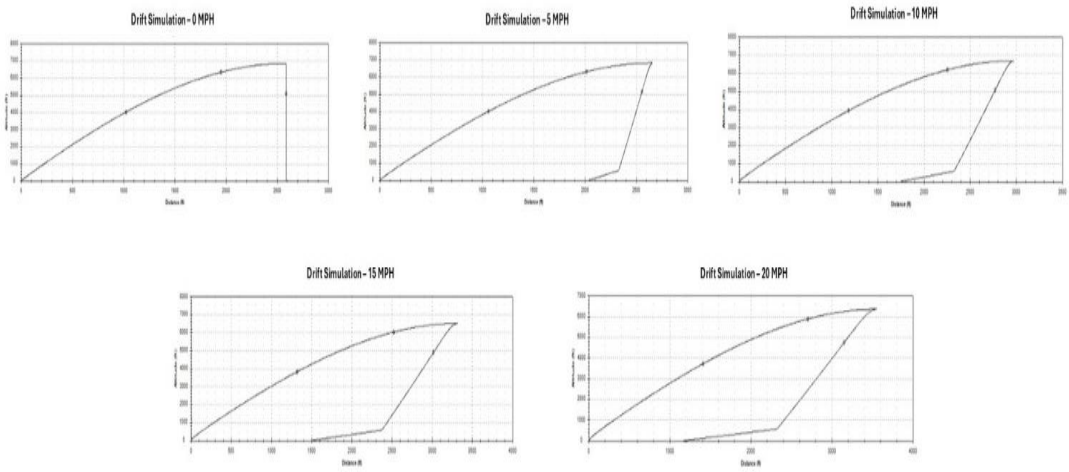

Figure 3.5.8: RASAero altitude over lateral distance simulations at winds speeds from 0-20 MPH by increments of 5 MPH

The OpenRocket and RASAero II simulation yielded similar trends, but different data. The RASAero II data was higher than the OpenRocket simulation data for lateral distance, which is likely due to how each software calculates and simulates the data. Additionally, all simulations, except for the 0 MPH, showed the rocket landing within the 2500 ft radius. Because the 0 MPH simulation showed it rocket traveling further than 2500 ft, the simulation was run again, but with a decreased launch angle. The launch angle was lowered to 5 degrees, which is the angle that will likely be used, rather than 10 degrees, which is upper limit for the launch angle. The 0 MPH simulation was run, and the data showed the rocket landing within the desired radius.

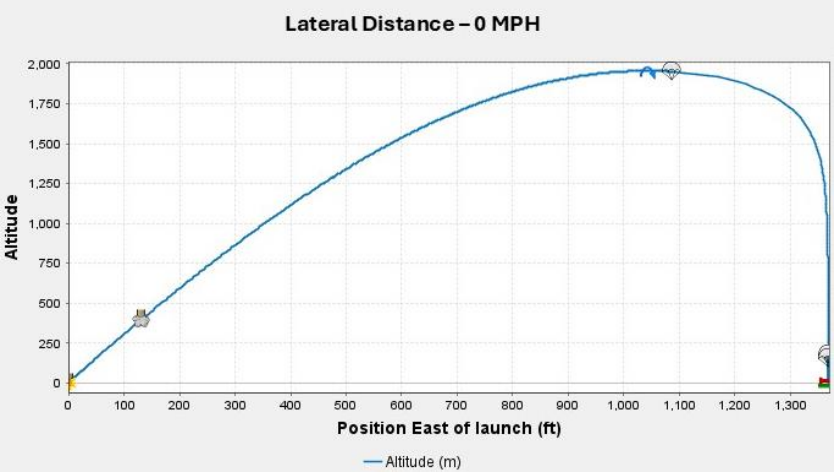

Figure 3.5.9: OpenRocket altitude over lateral distance simulation for 5 degree launch angle with 0 MPH wind

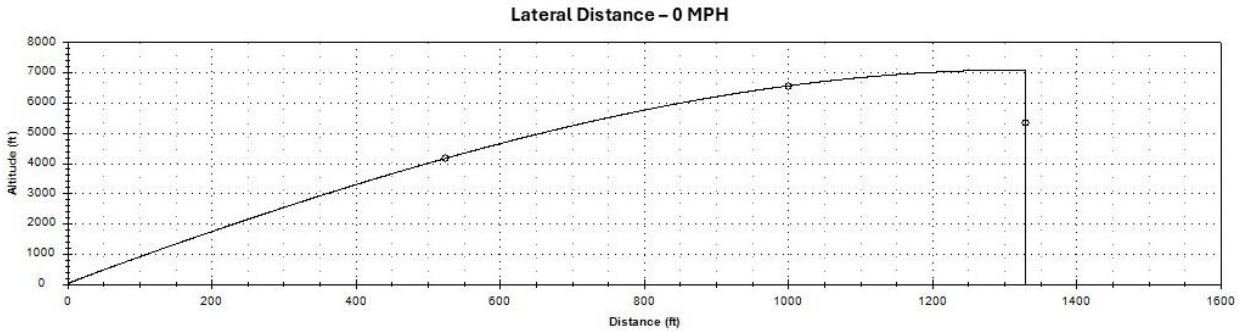

Figure 3.5.10: RASAero II altitude over lateral distance simulation for 5 degree launch angle with 0 MPH wind

4 Payload Design

4.1 Payload Criteria

4.1.1 Mission Statement

4.1.1.1 Passive Electronic Recovery Reporting – Capsule

Passive Electronic Recovery Reporting (PERR-C) aims to aid and monitor the launch of our rocket alongside reporting on the NASA-outlined datapoints via two main methods of communication, one being our own ground station, and the other being the pre-determined two-meter radio outlined in the handbook issued at the onset of the competition. These datapoints would be the apogee of the rocket, maximum velocity, and time of landing, all generated via sensor inputs processed in Python, although we have accounted for more outputs from our sensor package in the event that they can be achieved with the time allotted for development. These datapoints will be communicated via two main methods, the first being a ~915MHz radio that will interface with a ground station built off a RP2040 microprocessor, outputting a text string generated by the on-rocket portion of our system to the serial display of either a laptop, or other compatible device. The second means of communication will occur over the two meter (~144MHz) band, and interface with the control station listed in the handbook via audio, outputting a TTS version of the text string generated by the on-rocket portion, or some equivalent means of transmission if our chosen method is found to be not optimal during testing later in the year.

4.1.1.2 Altitude Control System

The Altitude Control System (ACS) aims to meet NASA requirements to reach a target altitude for better scoring in the competition by use of an inflight airbrake system. Functionally, this system bears immense resemblance to the PERR-C section of our craft, but differs primarily in regard to the peripherals it interfaces with. The sensor package and processing hub are identical to the aforementioned computer, but instead of broadcasting its processed data out to various remote components of our system, the ACS drives a motor that acts as the primary source of motion in the rocket's airbrake system.

4.1.2 Mission Success Criteria

4.1.2.1 Passive Electronic Recovery Reporting – Capsule

PERR-C is considered a success if all subsystems power on and communicate successfully with both the ground station and the NASA radio, allowing for successful monitoring and recovery alongside an accurate output of collected data to the Judges. This is combined with the criteria of keeping the STEMnauts safe and "alive" after landing. PERR-C must be able to function properly after landing with none of the mechanical or electrical components broken.

4.1.2.2 Altitude Control System

ACS is considered a success if the system recognizes the desired deployment altitude for the airbrake and engages the motor with enough lead time to make sure Peregrine Explorer does not overshoot the target altitude. It also needs to be able to react to the change in velocity, acceleration, and altitude to feather the airbrake effectively.

4.2 Passive Electronic Recovery Reporting – Capsule

4.2.1 PERR-C Design Process Alternatives

The PERR-C payload has undergone numerous variations during the design process, including both the electronics and mechanical design systems. Alternative mechanical designs for PERR-C looked at changing the number of sections of the nosecone, relocating the parachute eyebolt to better fit NASA mission requirements, STEMnaut visibility, nosecone section joint methods, and material choices for increasing strength and manufacturability. Alternative computer designs for PERR-C looked at microcontroller computing power, power circuit safety, code bases, and alternative sensor packages.

4.2.1.1 Alternate Mechanical Designs

The PERR-C System had multiple alternative solutions for different subcomponents throughout the design process. The external design for the nosecone underwent multiple design iterations, mostly consisting of how to introduce a transparent section to allow for the STEMnauts to have visibility on the flight deck.

The first iteration of this nosecone utilized a four-section design in which the upper portion of the nosecone was made from three different pieces, an opaque base, a central translucent ring, and an upper opaque tip, whilst the fourth section was the opaque base. The three upper sections would be fused together either through utilizing dual-extrusion FDM printing or threaded fixtures and adhesive, while the upper portion of the nosecone would be connected to the base through a threaded base. Ultimately, this design was decided against due to the added complexity of using multiple different additional sections which added unnecessary points of failure to the design.

The next iteration explored using a similar design but with three sections instead of two, the opaque base, clear mid-section, and opaque tip. This idea was decided against for similar reasons to the original design, including unnecessary added points of failure and manufacturability concerns. The next factor which was looked at was the material to be used for the translucent section of the nosecone. The original design called for clear resin using SLA manufacturing to ensure a truly clear part, however this solution was decided against due to the fragile nature of resin prints, the expense of manufacturing clear resin, and the potential issues with interfacing resin parts with traditional FDM components. The second alternative consideration was to remove the transparent component entirely, however this eliminated visibility for the STEMnauts and therefore was considered an unreasonable choice as a result.

An additional consideration was to do a two-piece design with a full transparent upper section made from PETG and an opaque PLA base, utilizing a screwed interface between

the two parts. Additionally, this design would employ masking off clear sections and painting over the transparent plastic to provide opaque sections without having to add interface points and therefore unnecessary points of failure to the design. This design poses potential issues with manufacturability however, including paint drips and adhesion to the plastic.

An alternative design consideration for the nosecone joints was a bayonet style joint to lock the base and upper portion together, however this poses manufacturability concerns and potential issues with the final security of the structure. Another design consideration was the placement of the eyebolt which attaches to the shock cord and rocket recovery system. The original design had the eyebolt at the top of the internal nosecone geometry above the PERR-C computers and STEMnauts, with the chord running externally along the side of the nosecone and re-entering the rocket body below the PERR-C system, where the parachute was packed. This design was later determined to potentially not align with the NASA mission requirements, and therefore was altered to place the eyebolt below the PERR-C system on the bottom of the nosecone, at which point it will interface with the rocket recovery system.

4.2.1.2 Alternate Computer Designs

While some variation was encountered in ideal designs regarding each team member's desires for the final implementation of the computer, much of this variation was tangential, affecting mainly the internal workings of the processors and sensors, rather than the layout of the device itself. Initially, alternate microprocessors were considered, including those in the STM32 and AT Mega product line, mainly due to familiarity, and the density of each respective package, allowing for the device to be fully integrated into a singular board rather than the "Arduino shield" style solution that currently exists. In the end, this layout was discarded after being weighed against the Feather S3. The team reached the conclusion that this device contained much more utility in a package that was not significantly larger than either of the AIO solutions proposed.

Adafruit boards such as the Feather eventually became a prime factor in deciding much of our component selection for the computer. Since this project requires a high degree of sensitivity regarding collected data for optimal operation, most of the sensors we will be working with are small, surface mount components that are difficult to interface with common prototyping methods. The breakout boards supplied by various manufacturers, and the availability and open-endedness of such devices, determined whether or not we'd have ample development resources to confidently be able to implement a given IC. This was the reason for the discarding of the MPU9250, among other scrapped chip options.

The potential for multithreading was accounted for in the design, with the communication and storage breakouts existing on a separate bus from our sensor package, meaning that both relevant sections of the hardware could be hypothetically interfaced with by each core within the ESP32, but any further accommodations to that layout were discarded by the software development team shortly into initial testing with the breadboarded prototype. More attention was needed regarding simply generating reliable, timely, and

accurate outputs from the on-rocket portion, therefore “hardware acceleration” of that process would be lowered in priority until such was achieved.

Several options were considered for fulfilling the 2-meter radio requirement set forth in the handbook. Initially, investigations regarding our solution focused on hunting down packet radios that would be functionally analogous to our 900MHz monitoring solution. Several out-of-production chips were found, and an attempt to source these parts was made to little avail. Had these components been included in our design, they would have communicated over one of the two commercial communication standards already present within the flight computer, and likely would have relied upon a ground up code library developed by the team.

4.2.2 Selected PERR-C Subsystem Design

4.2.2.1 Mechanical Hardware Design

The selected mechanical design for the PERR-C system utilizes a two-section nosecone design consisting of a Polylactic Acid (PLA) base and a Polyethylene Terephthalate Glycol (PETG) upper section. Both sections will utilize Fused Deposition Modeling (FDM) to manufacture, which allows for a high level of control in the design process, rapid development and iteration, and the ability to create complex internal geometries not otherwise possible through traditional methods. The upper section will specifically use Clear PETG as the material of choice, which will allow for increased visibility of internal components, as well as visibility for the STEMnauts on the flight deck, allowing them to monitor the landing site visibly alongside the electronics system. The floor of the flight deck will be a plywood bulkhead which will also act as the holding point for the primary threaded rod that holds PERR-C together. Below the flight deck will sit the electronics bay where the flight controller and sensor packages are held. At the bottom of PERR-C is the lower plywood bulkhead which acts as the lower holding point to which the eyebolt is fixed that attaches the capsule to the rest of the rocket and the recovery system.

The benefits of this design are primarily in the flexibility and ease of manufacturing that it offers. By utilizing a two-piece design for the nosecone, the points of failure are minimized whilst maintaining access to the flight deck. Using plywood as the bulkhead material allows for cheap and rapid manufacturing as well as increased thermal resistance when compared to PLA bulkheads. Using bulkheads as a separate article from the rest of the nosecone base allows for easy accessibility to the rest of the nosecone internals for installing and configuring the PERR-C computers. The upper portion of the nosecone being made from PETG offers increased thermal and stress resistance over a traditional PLA design.

4.2.2.2 Computer Hardware Design

Name of hardware	Function
Adafruit ESP32-S3 Feather	Flight controller
BMP388	Low accuracy barometer
ADXL375	High g accelerometer
ICM-20948	Inertial measurement unit/gyro
RFM69HCW	915 MHZ transceiver
MP3115A2	High accuracy barometer
SPI Flash SD Card (Adafruit)	SPI flash card
PA1010D	GPS module

Table 4.2.1: List of hardware for payload computer

		ESP32-S3 Feather+BMP388+ADXL375+ICM20948	Teensy 4.1+BMP388+ADXL375+ICM20948	ATSAMD21E16L+LPS22HB+MPU9250
Factors	Weighting	Score	Score	Score
Price	0.1	9	6	8
Accuracy	0.25	8	7	6
RAM	0.15	10	5	2
Flash Memory	0.1	9	9	2
Speed	0.1	8	10	6
In stock with manufacturer	0.05	1	1	0
Experience with components	0.25	9	6	5
FINAL WEIGHTED SUM		8.4	6.55	4.65

Figure 4.2.1: Decision matrix for hardware packages

The Payload Electronics team considered 3 main configurations of the computer system and finalized the green highlighted design option after carefully weighing all hypothetical layouts. Out of the various processors presented for the central hub of the on-rocket portion of our system, the ESP32 based Feather S3 from Adafruit was selected due to the bump in computing power over its counterparts, the inclusion of some basic power connectivity and safety circuits, and the integration of certain wireless communication methods into the processor, allowing for retroactive code changes to be enacted upon the device without physically interfacing with it, something that may serve beneficial as the final launch approaches and the rocket can no longer be fully deconstructed. The employment of this “brain” lessens the scope of what will be explicitly required on our “shield” and gives us a separate base of user experience if complications are encountered during the design and testing of our device.

The BMP388 was chosen as the barometer for the device due to prior experience with the sensor from previous years projects, as well as the ease of connectivity and the pre-existing base of code available online for the team to build off. There was some concern regarding the varied availability of the part depending on our chosen PCB manufacturer, but similar, newer sensors were found to be available from Bosch that utilized either an identical or similar base of code and package design. Similar justifications were reached for most other layouts of the computer, with the main concerns voiced by the team being the interchangeability of the various processors if massive complications were encountered during development or testing. A redundant barometer, the MP3115A2, is included in our design for redundancy and higher precision. The ADXL375 was chosen due to the low cost of the development board, and its integration into the CircuitPython library, both of which have accelerated our development process. The RFM69HCW is a SPI

enabled packet radio that will serve as our go between with the on-rocket portion of the system for mid-flight monitoring, alongside enabling and disabling the 2-meter radio connection as needed. All chosen sensors interface with the processing hub via either I2C or SPI, and the current prototype that exists currently has ample space for further connections of other devices compatible with these connection methods.

The two meter radio solution settled on by the team utilizes a compact commercially available radio module that features a semi-standardized communication method that interfaces over a 3.5mm and 2.5mm jack. These jacks will be split open into individual wires and hooked up to the associated analog and digital output pins as needed. The essential connections within this cable are the audio outputs for our text-to-speech system, and the digital enable/disable channel for the radio itself.

		Python	Arduino
Factors	**Weighting**	**Score**	**Score**
Ease of Programming	0.15	9	7
Libraries	0.25	8	8
Development Environment	0.15	10	5
Scalability & Flexability	0.1	9	6
Fault Tolerance	0.2	8	7
Real-Time Processing	0.15	2	8
FINAL WEIGHTED SUM		7.65	7

Figure 4.2.2 Decision Matrix for Selecting Coding Language

Similarly to the hardware configuration we also considered 2 main code bases, either CircuitPython or Arduino. CircuitPython was ultimately decided on due to processing speed and familiarity. In the state that the prototype currently exists in, there is little need to deviate from the common implementation of most sensors and hub-interfacing devices code-wise, meaning that the high-level language that is Python is a better fit regarding getting the system up and running. Beyond this, the availability of the lower-level C++ code that enables the CircuitPython libraries will enable swapping to a more involved coding language if such a transition benefits the project. Most of the modules selected for use on the flight computer have equivalent code bases in C/Arduino IDE. As of the time of writing, very little currently exists in the way of reportable, tangible code due to delays in the hardware prototyping process. The consensus among the team for that eventual design is to try and separate out the portions of our software that are responsible for interfacing with the sensors as much as we can from any other needed tasks, allowing for high rates of data input and processing without holding up peripherals, or other external processes.

4.3 Altitude Control System

4.3.1 Overview

The Altitude Control System (ACS) is designed to provide finer control over the launch vehicle's altitude to increase the team's apogee score. The ACS subsystem includes the mechanical system, control software and a dedicated guidance, navigation and control computer (GNC).

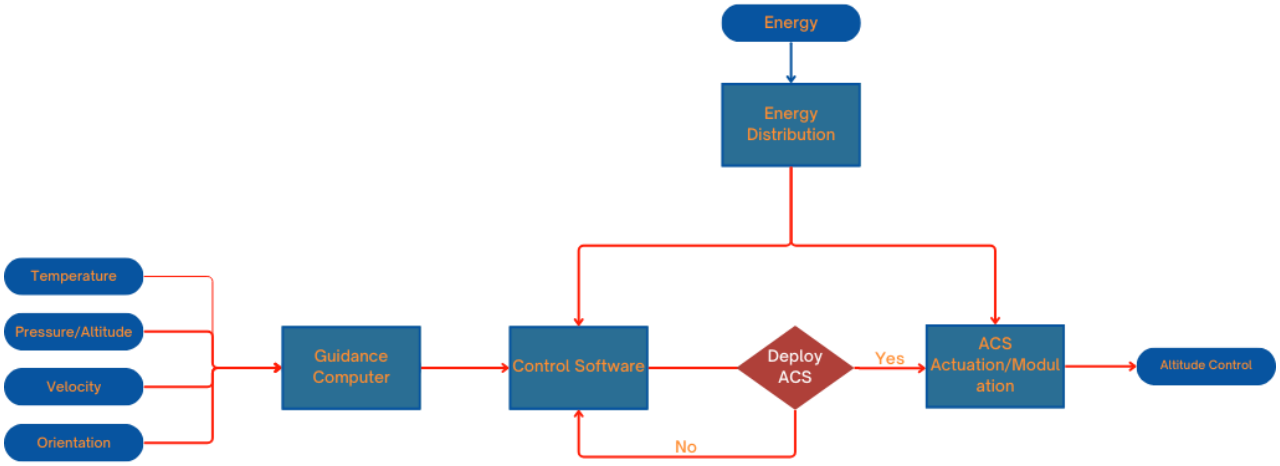

Figure 4.3.1 ACS Function Flow Diagram

Figure 4.3.1 demonstrates the abstract functional flow of the ACS subsystem. The GNC monitors telemetry and responds once in-flight state begins. The onboard control software determines if motor burnout has occurred and upon burnout detection the software activates its modules to calculate control inputs. If the software then further determines that the vehicle stability meets safety standards, it controls the ACS braking effect through the mechanical subsystem.

4.3.2 ACS Design Process Alternatives

4.3.2.1 Alternate Mechanical Designs

As part of the design iteration for the ACS, several concepts were considered to optimize the deployment of aerodynamic surfaces responsible for controlling drag. The primary design objective for the mechanical system was to maximize reliability and actuation speed. This is crucial because drag force increases with the square of velocity. A rapid deployment ensures that the ACS can take advantage of the high drag forces present at higher velocities during flight. By achieving full deployment quickly, the ACS maximizes its effectiveness in reducing the rocket's altitude. In addition to deployment speed, another key factor was the simplicity and reliability of the mechanical components. The system needed to be durable, able to perform consistently under high aerodynamic loads, and minimize failure points. Below is a comparison of the mechanical systems considered:

	Speed	Control Precision	Weight	Load Capacity	Safety Potential	Power Compatibility	Cost	
CRITERIA DESCRIPTION	Actuation Time: <1s	Modulation Precision: ± 0.3°	Weight: <700g	Holding Torque: >35N * cm	Minimum Failure Points? (Y/N)	Lower Voltages preferred	Affordable? (Y/N)	
								WEIGHTED SCORE
WEIGHT	0.2	0.25	0.05	0.2	0.1	0.1	0.1	1
	20%	25%	5%	20%	10%	10%	10%	100%
OPTIONS	Score	Score	Score	Score	Yes = 10, No = 0	>9V = 0	Yes = 10, No = 0	
Nema 17 Stepper + 2mm Pitch Lead Screw	8	10	10	10	10	8	10	9
775 DC 12 -24V (12000 RPM) + 2mm Pitch Lead Screw	10	2	10	6	10	0	10	6
NEMA 17 Stepper + Steel Geared Actuation	10	10	10	2	0	8	10	7

Table 4.3.1 Decision matrix of ACS mechanical subsystem core components

As shown in Table 4.3.1, the ranked design criteria included metrics for actuation time, control precision, load capacity, power requirements, safety, cost, and system weight. These stringent guidelines enabled the ACS to be equipped with a robust mechanical subsystem. The resulting choice was a combination of a stepper motor and a linear lead screw mechanism. The stepper motor's ability to handle high torque loads during ACS operation ensures mechanical rigidity even under significant aerodynamic forces. Additionally, its precision allows for rapid and accurate deployment.

In contrast, the other two concepts—a DC motor paired with a lead screw and a gear-based system—were less viable. The DC motor system lacks the required holding torque demanded by our safety factor and fails to provide the minimum torque necessary to maintain a rigid deflection angle. Furthermore, it lacks the control precision that the stepper motor offers. A gear-based mechanical design introduces potential points of failure and slippage due to the compact size requirements of the flap linkages. Additionally, the gear design would be more challenging to manufacture given the current aerodynamic concept of the ACS flaps.

4.3.2.1.1 Lead Screw Selection

The selection of the lead screw was critical to achieving these objectives. After evaluating various options, an 8mm diameter lead screw with a screw pitch of 2mm and a lead of 8mm was chosen. The lead screw has a length of 300mm which will be cut down to length during the building process.

Lead Screw Specification	
Diameter	8mm
Screw Pitch	2mm
Lead	8mm
Length	300mm
Material	High-strength stainless steel
Thread Type	Trapezoidal ACME threads

Table 4.3.2 ACS Mechanical Subsystem: Lead Screw component specification

Reasons for Lead Screw Selection:

- Mechanical Robustness: Thick threads and ACME profile that has offers a greater surface contact area, which helps distributing loads and reduces stress concentrations
- Efficient Linear Motion: A high lead length of 8mm allows for increased deflection of the flaps while reducing the number of revolutions required to get there.
- Precise control: A fine screw pitch of 2mm allows for precise control and high repeatability over control surface
- Ease of procurement: This lead screw is commonly used in high stress 3D printing applications and is easy to acquire through commercial means

4.3.2.1.2 Motor Selection

For actuating the lead screw, a 42-34 stepper motor was selected after thorough analysis of the torque, speed, and precision requirements.

NEMA -17 Stepper Motor Specification	
Frame Size	42 mm x 42mm
Length	34 mm
Step Angle	1.8 ° per step (200 steps/rev)
Holding Torque	48 N·cm
Max Speed	1000 RPM
Rated Current	1.7A per phase
Voltage	5V-12V
Number of Phases	2
Drive Method	Bipolar
Shaft Diameter	5mm
Detent Torque	2.5Ncm

Table 4.3.3 Mechanical Subsystem: Stepper Motor component specification

Reasons for Motor Selection:

- High Torque Output: The NEMA-17 spec chosen offers 48 N·cm of holding torque, this is adequate to handle the drag loads across the surface of the flaps of the ACS
- Precision and Control: The 1.8° step angle coupled with a motor driver capable of micro stepping allows for 10,000 steps/rev. When coupled with the precision lead screw this allows linear resolution of 0.02mm
- Speed Requirements: 1000RPM is sufficient to meet actuation speed requirements
- Electrical Compatibility: The motor operates at a flexible range of voltages from 5-12V, this allows for better compatibility with existing batteries onboard.

4.3.2.2 Alternate Aerodynamic Designs

From the initial conception, the aerodynamic design of the ACS was focused on maximizing surface area to effectively disrupt free-flowing air and generate significant drag. This design philosophy allowed for rapid conceptualization and prototyping, leading to the quick elimination of concepts that failed to meet surface area requirements. Among the discarded designs were several geared mechanisms featuring flower petal-like extensions intended to generate drag. While these designs were conceptually intriguing, they were ultimately abandoned due to their inability to provide adequate surface area for effective altitude control.

The original design concept involved 2 hinged cross-sectional flaps of the vehicle's body tube, which would open to interfere with the airflow and create drag. The figure below provides a rough illustration of the early design.

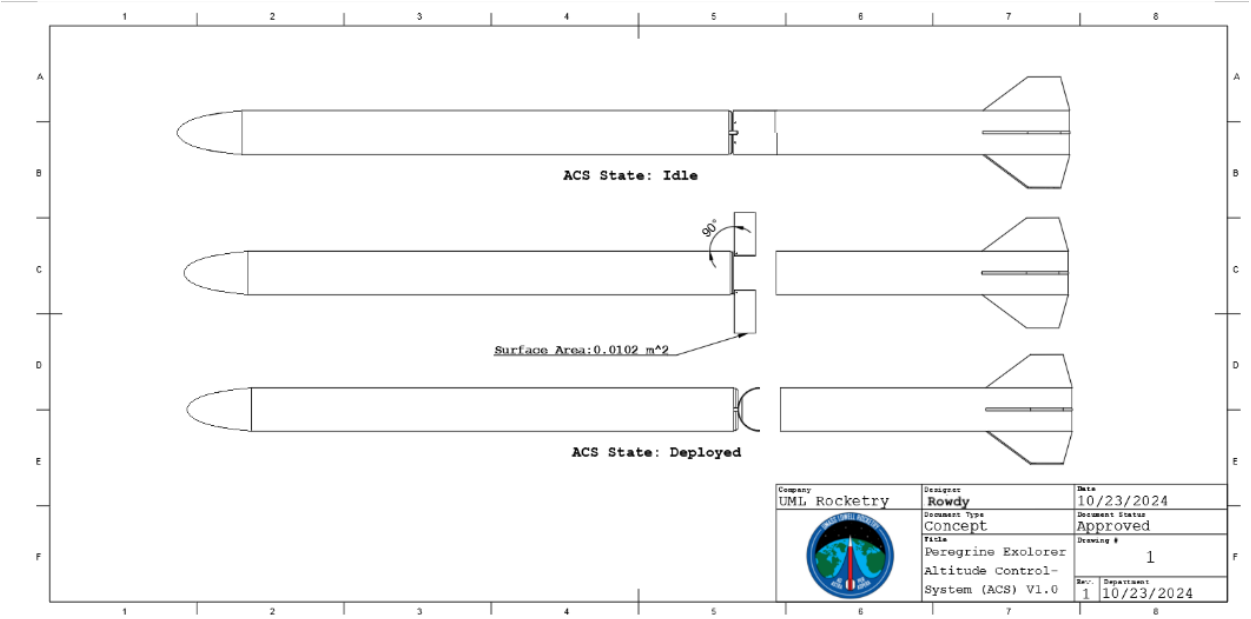

Figure 4.3.2 Initial design concept of ACS on Peregrine Explorer full scale vehicle

Figure 4.3.2 illustrates the ACS in its two operational states: idle and deployed. The top model shows the flaps closed, which is the system's state during powered flight and in the event of any concerning anomalies. The deployed state displays the ACS fully extended at 90 degrees. Note that the flaps can also be deployed at discrete angles between 0 and 90 degrees.

4.3.3 Selected ACS Subsystem Design

4.3.3.1 Computer Hardware Design

Initial designs for the control hardware for ACS considered a through-rocket cable connected to a breakout board that would house all relevant chipsets and components responsible for driving the stepper motor for the airbrake. Upon further discussion with the other subsystems teams, this concept was scrapped for a variety of reasons. Chief among these, the length and pathway for this wire introduced immense opportunities for complete electrical failure within the airbrake. While the power source for the motor would be housed within ACS, the hypothetical data cable would span much of the rocket's vertical length and require overhauls and considerations from other subsystems to be feasibly implemented. Instead, we recognized that the payload flight computer would inherently be operating within failure rate margins that made replicating the device in a separate section of the craft irrelevant to the reliability of the overall device. Therefore, the hardware driving ACS is an exact replication of the processing hub and sensor package for PERR-C, with a different PCB shape and peripherals attached to it. Accommodation for high voltage LiPo terminals will be made within the PCB, and the Toshiba TB6612FNG will be added to the layout to enable microprocessor-motor interfacing. Two power sources will be present within the system, one for the driver circuits, and another for the logic level circuitry.

4.3.3.2 Control Software Design

The control software for the Altitude Control System (ACS) is a pivotal component that ensures the rocket achieves its target apogee with precision while maintaining optimal flight stability and safety. It is engineered as a closed-loop feedback control system that dynamically adjusts the deployment of the airbrake flaps based on real-time telemetry data. This leverages inputs from multiple onboard sensors, including the Inertial Measurement Unit (IMU), barometric pressure sensors, and GPS, to make informed decisions during the flight.

4.3.3.2.1 Primary Software Modules

Data Acquisition: Real-time collection of sensor data (IMU, barometric sensors, GPS).

Altitude Control Algorithm: Continuous computation of altitude, velocity, and drag force to adjust airbrake deployment.

Deployment Control: Commands for actuating the lead screw and motor to control the position of the ACS flaps.

Safety System Override: Real-time monitoring of flight conditions, ensuring that safety protocols are followed in the event of anomalies or system failures.

4.3.3.2.2 Software Architecture

The ACS control software is structured into several interconnected modules, each serving a specific function within the system. The primary modules include:

- Data Acquisition Module
- State Estimation Module
- Apogee Prediction Algorithm
- Control Law Computation (PID Controller)
- Deployment Control Module
- Safety and Fault Management Module

4.3.3.2.2.1 Data Acquisition Module

The Data Acquisition Module is responsible for collecting real-time data from various sensors critical to the control algorithms. It interfaces with:

- Inertial Measurement Unit (IMU): Provides high-frequency acceleration and angular velocity data.
- Barometric Pressure Sensors: Offer altitude measurements based on atmospheric pressure variations.
- GPS Receiver: Supplies precise positional data and serves as a redundancy check for altitude and velocity.

This module incorporates signal conditioning and filtering techniques to mitigate noise and improve the reliability of sensor data. It ensures synchronized data sampling to maintain the temporal integrity of the measurements.

4.3.3.2.2.2 State Estimation Module

The State Estimation Module processes the raw sensor data to derive accurate estimates of the rocket's current state parameters:

- Altitude
- Vertical Velocity
- Acceleration
- Attitude (orientation in pitch, yaw, and roll)

By employing sensor fusion algorithms, such as Extended Kalman Filters (EKF), this module enhances the accuracy of state estimates by combining measurements from different sensors and accounting for their respective uncertainties.

4.3.3.2.2.3 Apogee Prediction Algorithm

The Apogee Prediction Algorithm calculates the expected maximum altitude (apogee) the rocket will reach based on its current state and flight dynamics. The algorithm considers:

- Current altitude and vertical velocity
- Gravitational acceleration
- Aerodynamic drag forces

The prediction is continuously updated as new data becomes available, allowing the control system to adjust airbrake deployment proactively. The algorithm uses numerical methods to solve the equations of motion, accommodating non-linearities in drag and atmospheric conditions.

4.3.3.2.2.4 Control Law Computation (PID Controller)

At the heart of the control software is the Control Law Computation module, which utilizes a Proportional-Integral-Derivative (PID) controller to determine the necessary adjustments to the airbrake flaps. The PID controller works to minimize the error ($e(t)$) between the predicted apogee and the target apogee by calculating a control output ($u(t)$):

$$u(t) = K_p \boldsymbol{e}(t) + K_i \int_0^t e\,(\tau)d\tau + K_d \frac{de(t)}{dt}$$

Where:

- $\boldsymbol{K_p}$ (Proportional Gain): Reacts to the current error magnitude.
- $\boldsymbol{K_i}$ (Integral Gain): Addresses accumulated past errors to eliminate steady state offset.
- $\boldsymbol{K_d}$ (Derivative Gain): Anticipates future errors based on the rate of error change.

4.3.3.2.2.5 Deployment Control Module

The Deployment Control Module translates the control output from the PID controller into physical actuation commands for the airbrake system. It manages:

- Stepper Motor Control: Sends precise step and direction signals to the motor driver, facilitating accurate positioning of the airbrake flaps via the lead screw mechanism.
- Position Feedback Integration: Monitors the position of the flaps using encoders or potentiometers to ensure the commanded position matches the actual position, enabling closed-loop position control.
- Synchronization: Coordinates multiple airbrake actuators to deploy symmetrically, preserving aerodynamic balance and preventing induced roll or yaw.

This module also incorporates motion profiles to smooth out actuator movements, reducing mechanical stress and extending the lifespan of the hardware components.

4.3.3.2.2.6 Safety and Fault Management Module

Safety is a paramount consideration in the control software design. The Safety and Fault Management Module implements various protocols to detect and respond to anomalies:

- Stability Checks: Before and during airbrake deployment, the software assesses flight stability by analyzing acceleration and angular rates against predefined thresholds.
- Fault Detection and Isolation (FDI): Continuously monitors system health, including sensor functionality, actuator performance, and communication integrity.
- Emergency Procedures: In the event of detected faults or unstable conditions, the module can inhibit airbrake deployment, retract flaps, or switch to a safe mode to prevent exacerbating the situation.
- Redundancy Management: Utilizes redundant sensors and pathways to ensure continued operation despite individual component failures.

4.3.3.3 Mechanical Hardware Design

The core mechanism of the ACS is driven by a stepper motor that is responsible for opening and closing the flaps. These flaps deflect outward while pivoting on a hinge attached to the forward bulkhead of the section, functioning similarly to an umbrella or the spoilers on an aircraft's wings, to create drag.

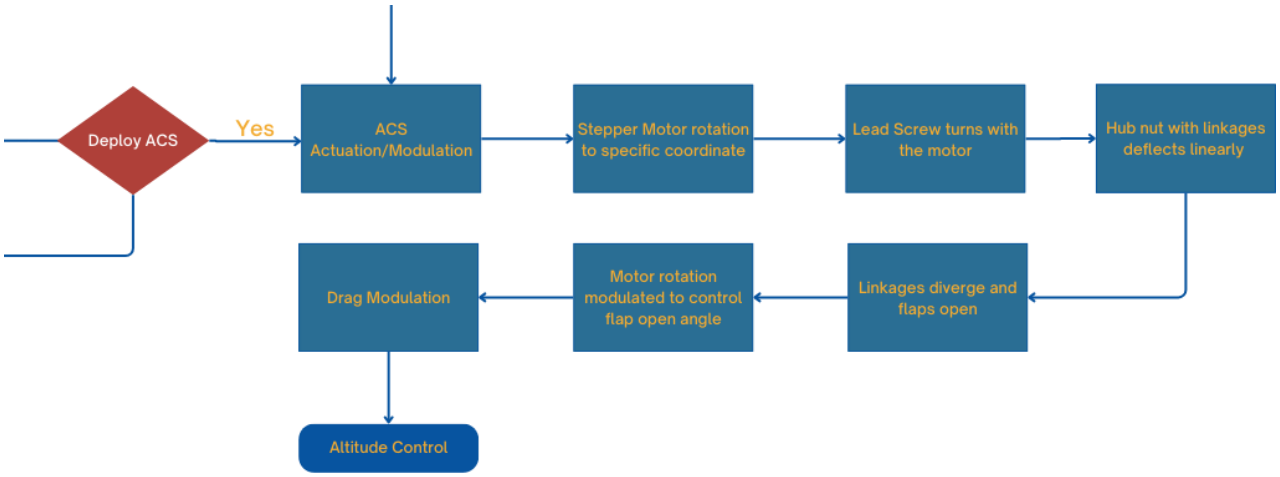

Figure 4.3.3 ACS mechanical function flow diagram

Figure 4.3.3 illustrates the mechanical flow diagram of the ACS. When the GNC system detects a flight state requiring ACS deployment, the stepper motor drives the lead screw, converting its rotational motion into linear motion of a threaded hub nut. This hub nut is connected to bushings that slide along a smooth ½-inch steel shaft, which serves as an intermediary load-bearing component to reduce the load experienced by the lead screw and stepper motor.

4.3.3.3.1 Mechanical Hardware Testing and Validation

Due to the current project timeline, real-world testing and validation of components are limited. In the future, more extensive testing will be conducted to analyze the load-bearing capabilities and real-world drag characteristics of the system. For now, however, the only available data pertains to the average deployment speed of the ACS. To obtain this data, repeated trials were conducted and timed. These trials included deployment ranges from 0–30 degrees, 0–60 degrees, and 0–90 degrees. Each deployment range was sampled three times, and an average was calculated to reduce noise and user variance.

	Trial 1	Trial 2	Trial 3	
angle	Time(s)	Time(s)	time(s)	Average Time(s)
0-30	1.3	1.02	1.04	1.12
0-60	2.3	2.5	2.2	2.333333333
0-90	3.1	2.9	2.8	2.933333333

Table 4.3.4 deployment speeds at different angles of stepper motor + lead screw core components

Table 4.3.4 presents an actuation matrix for the ACS, detailing the time required to transition from 0 degrees to specific discrete angles of 30, 60, and 90 degrees. On average, maximum deployment from 0 to 90 degrees is achieved in 2.9 seconds. To assess whether this actuation time provides adequate performance, the vehicle's vertical velocity 3 seconds after motor burnout was cross-referenced. This was done to ensure that the ACS could deploy quickly enough to capture additional drag force during high-velocity flight regimes, if needed.

To validate the effectiveness of the deployment timing, data from OpenRocket simulation was analyzed. Vertical velocity data ranging from t = Motor burnout to t = Motor burnout + 3.5s was exported and charted:

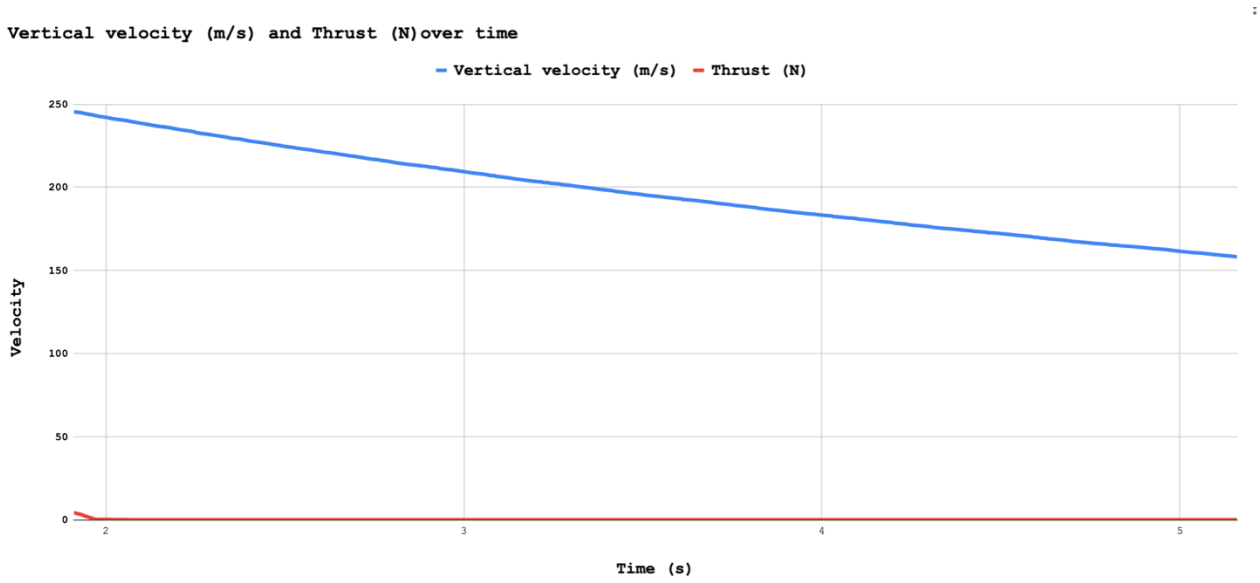

Figure 4.3.4 Vehicle Velocity immediately after motor burnout to mb +3s

Figure 4.3.4 illustrates the thrust and velocity right after motor burnout. At maximum deployment angle (Motor burnout + 3s), the vehicle approaches a velocity of approximately 160 m/s. Using this velocity and the preliminary design concept, an estimate of the total drag on the vehicle during airbrake deployment was made. To determine whether this deployment speed was sufficient, a preliminary drag force analysis was conducted using the base drag force equation.

$$F_d = \frac{1}{2}\rho v^2 \mathrm{A} C_d$$

To calculate the drag force transmitted to the vehicle by the airbrakes, a set of consistent assumptions was maintained throughout the simulation and analysis process. These assumptions are outlined below:

Assumptions		
Type	Value	Description
Nominal C_d of **BODY** without ACS deployed	0.0051	This is the C_d of the vehicle without the ACS deployed. Extracted from an average from CFD and OpenRocket data
Geometry of ACS Flaps	Flat Plate	This is an assumption made to get a reference drag value of just the airbrake. It allows for easy calculation of how much the addition of this airbrake will change the flight dynamics.
Nominal C_d of **ACS FLAP fully deployed [90 deg]**	1.2	This value was used to get a simple reference value of drag caused by each ACS flap at speed
Density of fluid (Air)	1.204 kg/m3	This value was used in all simulations and calculations as the Density of air
Velocity at deployment	160m/s	This value was used to get a discrete reference of the max drag at deployment with opening delays accounted
Surface Area of **ONE ACS FLAP**	0.0102 m^2	This the area of a flat plat that is dimensionally similar to the vehicle. A = 102 mm x 100 mm

Table 4.3.3 Assumptions made to calculate the effectiveness *of ACS deployment speed delay*

Once a set of assumptions is established, the drag generated by the ACS flaps at the deployment velocity can be calculated. This calculation provides a clear understanding of the aerodynamic forces acting on the system and allows for an accurate assessment of the flaps' effectiveness in generating the required drag for altitude control.

Drag force generated by singular ACS flap at 160m/s

$$F_d = \frac{1}{2}(1.204Kg/m^3)(160m/s)^2(0.0102m^2)(1.2)$$

$$F_d = 188.63N$$

Double F_d to get Total Drag force with 2 ACS Flaps at 90 degrees:

$$Total\ F_d = 377.26N$$

Theoretical max drag if ACS was deployed instantly after motor burnout:

$$v = 256\ m/s$$

$$F_d = \frac{1}{2}(1.204Kg/m^3)(256m/s)^2(0.0102m^2)(1.2)$$

$$F_d = 482.9\ N$$

$$Total\ F_d = 965.8N$$

The extrapolation from the 3s ACS deployment demonstrates that the system is capable of exerting a significant amount of drag force on the vehicle. This drag force effectively decelerates the rocket. The calculation results convey that a 3s deployment is sufficient for the ACS to provide sufficient braking power for optimal altitude control.

4.3.3.4 Aerodynamic Geometry Design

The drag analysis presented above validates the further investigation of drag characteristics using a more complex method and an aerodynamic model that more closely resembles the design concept. To achieve a more accurate representation of the system's performance, multiple methods and simulation software were employed. These tools allowed for a better approximation of the ACS's real-world behavior and enabled a comparative evaluation of different design concepts, ensuring that the final design delivers optimal aerodynamic performance. This was done to solve a design problem presented by the structures team to identify which design for an ACS would be better suited to reducing total altitude and how that would translate to altitude performance. The structures team presented two designs for the ACS, seen below.

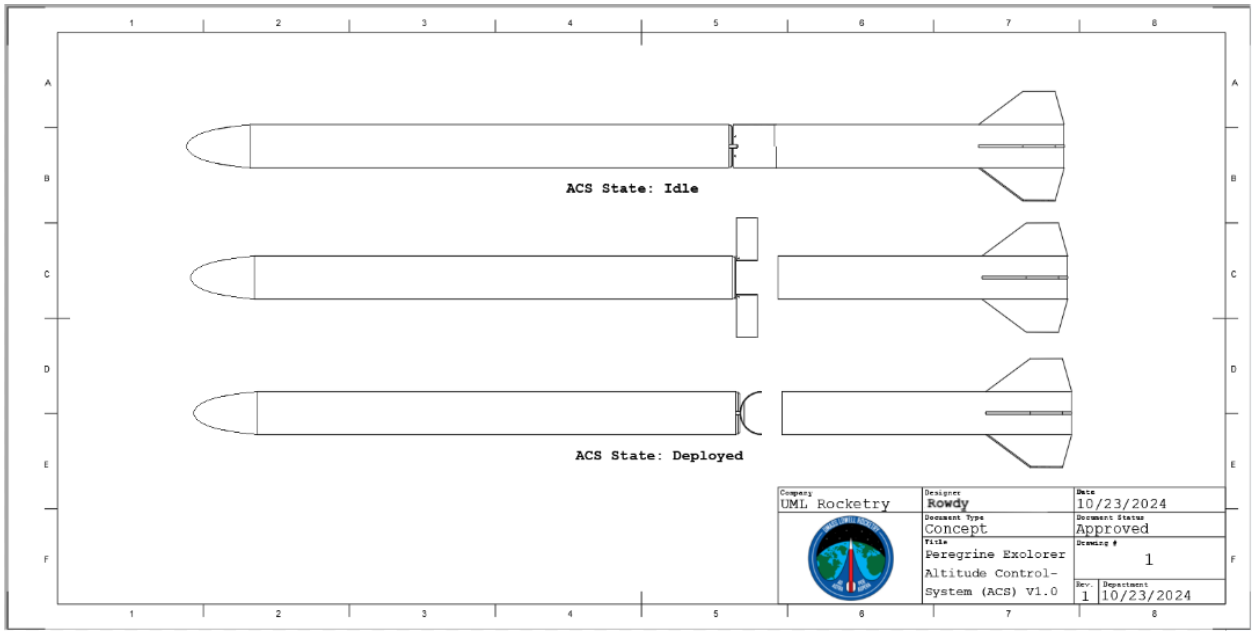

Figure 4.3.5 Forward opening ACS

Figure 4.3.5 displays the initial forward opening ACS concept. This design opens against the wind and offers a passive safety feature which is caused by the airflow pushing the flaps inward. In the case of mechanical failure or power loss, this system offers a safer mechanism for an airbrake.

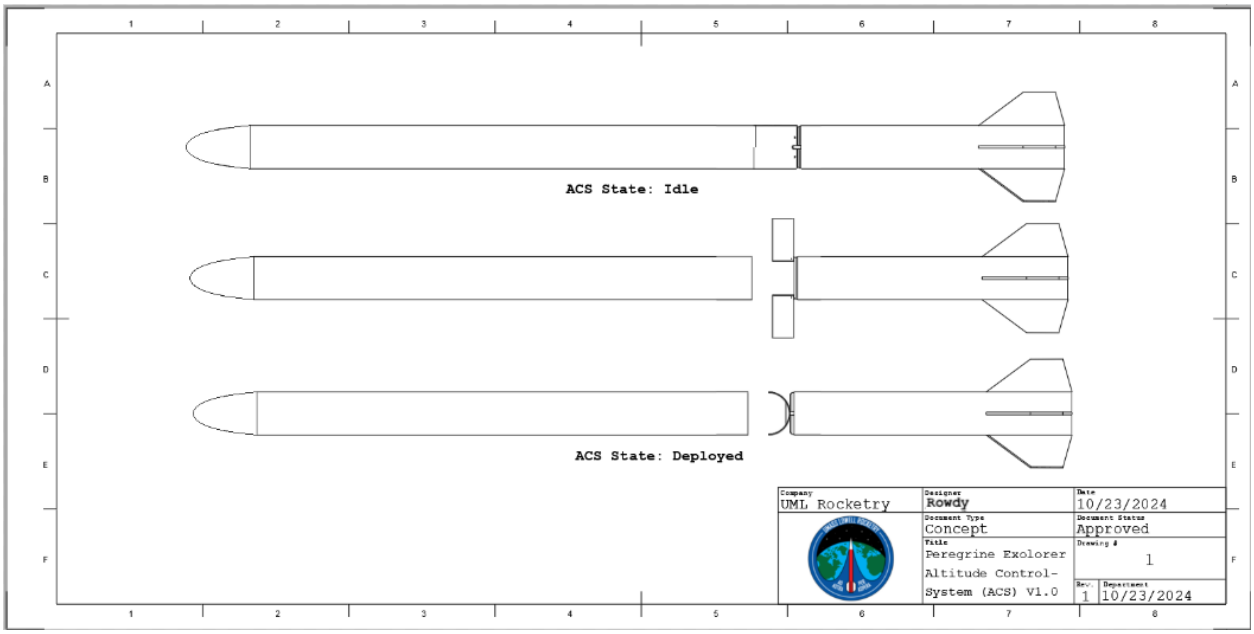

Figure 4.3.6 Reverse opening ACS

Figure 4.3.6 illustrates a reverse-opening ACS concept proposed as a potential optimization of the initial design to enhance braking performance. This design is hypothesized to generate increased drag force due to its concave flap profile that effectively "catches" the air, allowing the brake to transfer momentum more efficiently to the surrounding airflow.

However, despite its potential advantages, concave designs are generally discouraged for aerodynamic braking devices because they can trap air in a high-pressure zone known as a "bubble." This trapped air acts as a cushion, permitting the free-stream air to flow over the flaps and thereby reducing drag forces. This effect may be further amplified by airflow pooling within the ACS cavity when the flaps are at lower deployment angles. Nonetheless, these considerations are not conclusive and require validation through CFD analysis.

It is important to note that regardless of the performance outcomes, the vehicle will likely be equipped with the forward-opening design due to safety concerns associated with reverse opening, particularly in cases of power loss or mechanical failure.

4.3.3.4.1 Performance Analysis and comparison

The primary objective was to assess the performance outputs of alternative design concepts, with an emphasis on identifying a design that produces greater drag force. To achieve more accurate performance models, Computational Fluid Dynamics (CFD) simulations were proposed and selected as the analytical approach.

List of Software	
Software Name	Goal
OpenRocket	Reference values to compare CFD simulation accuracy and to calculate performance of ACS
Autodesk CFD Ultimate	CFD simulation of vehicle during ACS operation at varying opening angles and speeds
ANSYS Fluent	CFD simulation of vehicle to confirm validity of Autodesk CFD Ultimate
Google Sheets	Trajectory projection of vehicle with simulated ACS deployment

Table 4.3.4 List of software used to optimize ACS design

In this analysis, OpenRocket was used as a baseline reference to compare the results from CFD simulations. It was also employed to calculate the projected altitude using CFD data and kinematic equations. This approach was essential for validating the CFD data and developing reliable models for performance prediction, which will guide future developments of aerodynamic control schemes.

For CFD simulations, Autodesk CFD Ultimate was chosen due to its integrated workflow with Fusion 360. This integration allowed for rapid CFD setup, enabling extensive data collection and a more accurate assessment of performance across varying flight conditions and deployment angles. Due to concerns about the convergence criteria in Autodesk CFD, ANSYS Fluent was used as a validation check for two data points. The remaining simulations were assumed to be accurate since all simulations used mostly consistent environmental variables, bar a reference surface area value in Fluent.

4.3.3.4.2 Governing Equation

To properly set up the simulation, a governing equation for the physical model was established—the standard drag force equation:

$$F_d = \frac{1}{2}\rho \mathrm{A} C_d v^2$$

Establishing a governing equation allows for a validity check of the simulation results. The standard drag force equation can be used with drag forces from OpenRocket to calculate drag coefficients, which can then be compared to CFD results. This equation was also employed to assess preliminary designs, providing a rough approximation to identify any obvious significant issues with the results produced by the CFD simulations.

4.3.3.4.3 CFD Methodology and Results

Autodesk CFD played a critical role in the assessment and optimization of the ACS design. To obtain meaningful results from the CFD simulations, careful attention was given to the environment setup and boundary conditions. The accuracy and relevance of the results are highly dependent on the proper configuration of these variables. Knowing the equation that shall govern the simulation, assumptions could be made regarding the physical model. The assumptions are listed below:

Variable	Underlying Variation	Value
Density	Constant	1.204 kg/m^3
Surface Area (Not fully normal)	Constant	1.16947 m^2
Velocity	Constant	250 m/s
Deployment Angle	Constant	90 degrees
Iterations	Constant	500

Table 4.3.5 Setup variables for Autodesk CFD

These assumptions were made to simplify the model and focus on the primary characteristic of interest: drag force production. It was assumed that the air brakes would be fully deployed at a 90-degree angle and that this deployment would occur when the rocket was traveling at near-maximum speed. These assumptions were intended to simulate a "best-case" air brake scenario.

The rationale for this approach was that a design performing well in this scenario would likely perform better in other conditions, given the relationship between drag force and the coefficient of drag (Cd). Since both designs used the same components and differed only in the opening direction, the underlying principle was that a design generating more drag force would inherently create greater drag in all velocity profiles. However, this assumption ignores the process of opening the brakes, which will also need to be investigated to determine if prior states have any effect on overall performance.

Convergence:
The Autodesk CFD simulations were originally configured to run for 500 iterations. However, the built-in Convergence Monitoring feature in CFD Ultimate concluded the simulations earlier, at 448 iterations for the reverse-opening ACS configuration and 323 iterations for the forward-opening configuration. The difference in the number of required iterations, alongside a slightly more volatile convergence pattern for the reverse-opening design, indicates that the solver faced greater difficulty resolving the aerodynamic behavior for this configuration.

Despite this, the convergence graphs for both configurations flatlined and remained sufficiently stable, adhering to the established convergence criteria. The additional iterations required for the reverse-opening configuration are deemed negligible in terms of impact on the overall result. It is also important to note that the model orientation was flipped along the Z-axis for the forward-opening ACS during these simulations, although this does not affect the resulting data.

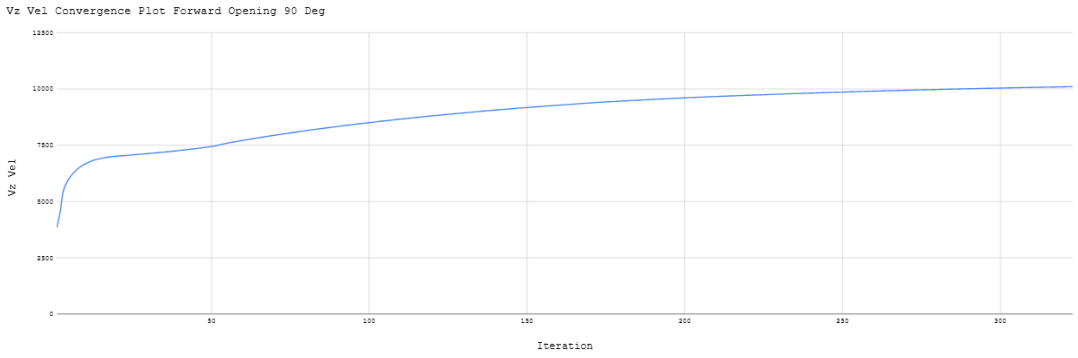

Figure 4.3.7 Velocity in Z axis Convergence Plot of Forward Opening at 90 Degrees Deployed

Figure 4.3.7 Shows a smooth convergence plot for velocity magnitude in Z-axis direction. The iteration counter was set to 500 but convergence was achieved in 328 iterations

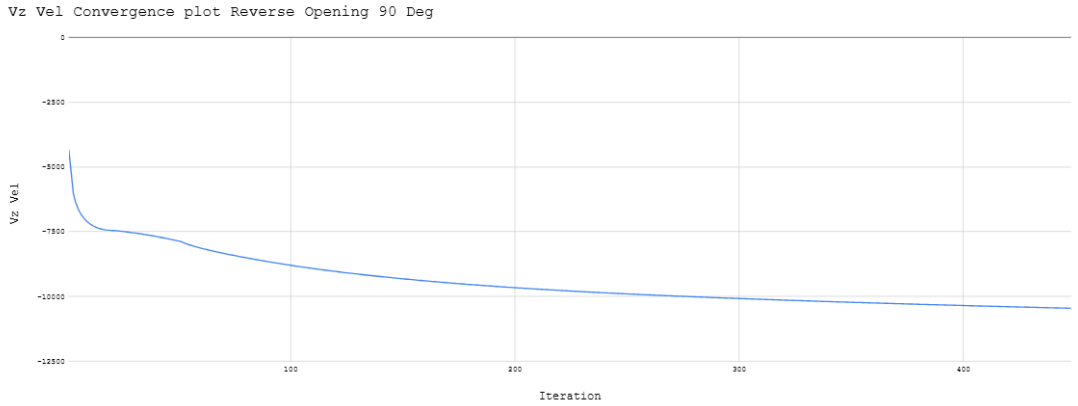

Figure 4.3.8 Vz Convergence Plot of Reverse Opening at 90 Degrees Deployed

Figure 4.3.8 Shows a smooth convergence plot for velocity magnitude in Z-axis direction. The iteration counter was set to 500 but convergence was achieved in 328 iterations

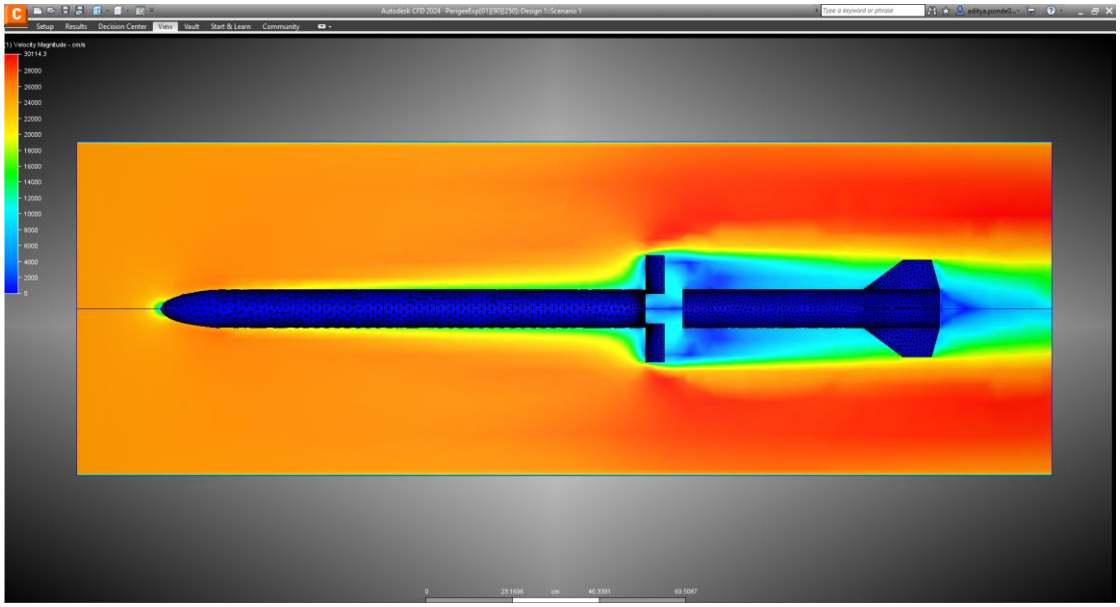

Figure 4.3.9 Forward opening velocity contour plot

The velocity contour plot for the forward-opening ACS design concept clearly illustrates the formation of a low-pressure zone as the airflow separates when passing over the deployed ACS flaps. This low-pressure zone is responsible for generating wake drag and contributes to turbulence in the surrounding flow due to the aerodynamic profile of the system. The simulation results indicate that this design produces approximately 1076 N of drag force at a velocity of 250 m/s, making it effective in reducing the rocket's velocity and controlling its altitude during the coast phase.

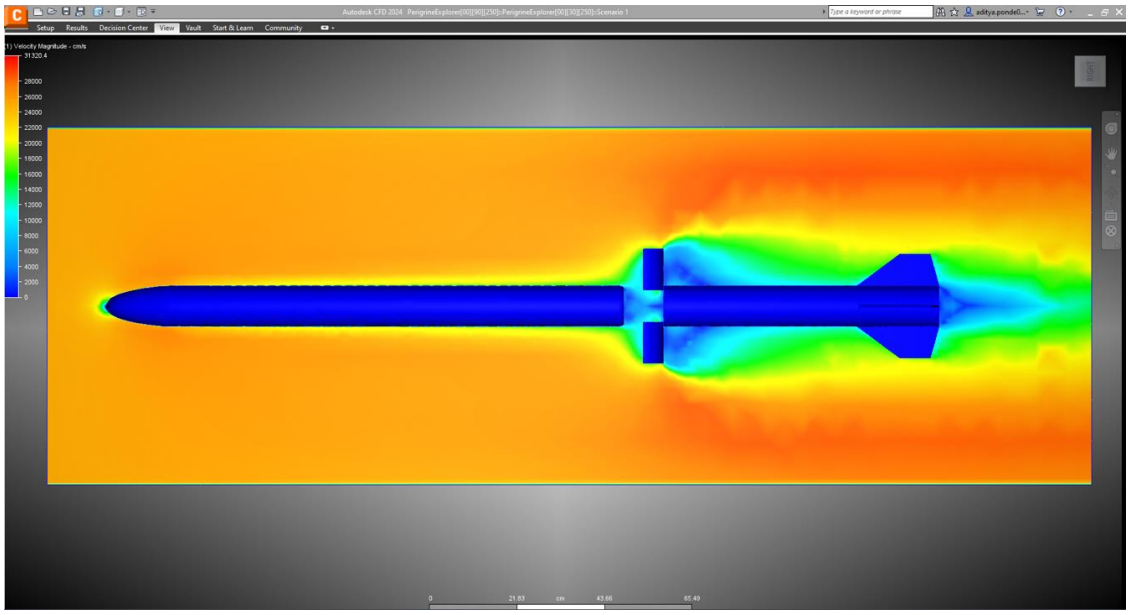

Figure 4.3.10 Reverse opening velocity contour plot

The velocity contour plot for the reverse-opening ACS design concept reveals a highly disturbed airflow pattern compared to the forward-opening configuration. A notable feature of this design is the high-speed airflow spilling over the outer edges of the ACS flaps, which leads to pressure concentration on the brake surfaces. This increased pressure contributes to the generation of 1501 N of drag force at a velocity of 250 m/s.

However, this design also increases the structural loads at peak velocities, raising concerns about the trade-off between additional drag and the potential safety risks due to higher stresses on the ACS components. It is critical that further Finite Element Analysis (FEA) and real-world testing be conducted to ensure that the net drag gain justifies the increased structural demands, particularly at high speeds.

Results:
The results of the Autodesk CFD Ultimate simulations are summarized in Table 4.3.6 below. Contrary to initial predictions, the rear-opening ACS did not perform worse due to the anticipated pocket of turbulent air forming within the body. In fact, under fully deployed conditions, the rear-opening ACS performed slightly better than the forward-opening ACS. Specifically, the drag force generated by the rear-opening ACS was 425 N

higher than that of the forward-opening ACS when tested under identical simulated conditions.

Quantity	Forward Opening	Rear Opening
Drag Force (N)	1076	1501
Coefficient of Drag	0.02445381809	0.03411262171

Table 4.3.6 Results from Autodesk CFD ultimate

These values indicate that, despite initial expectations, the forward-opening ACS generates less drag force compared to the rear-opening ACS. Initially, it was predicted that the rear-opening design would perform worse due to the formation of a turbulent air pocket within the cavity created by the flaps. This high-pressure zone, or "bubble," was expected to act as a cushion, reducing the effectiveness of the flaps in generating drag.

However, the simulation results suggest that the rear-opening ACS does not significantly suffer from this effect and, in fact, produces more drag. One possible explanation is that the concave profile of the rear-opening flaps effectively captures the airflow, increasing the drag force. The airflow dynamics may allow the rear-opening flaps to transfer momentum more efficiently to the surrounding air, enhancing the braking effect.

In contrast, the forward-opening ACS appears to lose some drag force due to its more aerodynamic profile and as indicated by the CFD contour plots.

Due to these unexpected results and the identification of convergence issues during the simulations, ANSYS Fluent was employed using consistent variables to validate the findings. ANSYS Fluent offers advanced meshing capabilities and more robust solver algorithms, which can address convergence problems and provide more accurate and reliable results. By cross-validating with ANSYS Fluent, confidence in the simulation data is increased, ensuring that the observed performance differences are not artifacts of the simulation software.

4.3.3.4.2 ANSYS Fluent Methodology and Results

Setup:

Variable	Constant?	Value
Density	Y	1.204 kg/m^3
Surface Area (normal)	Y	0.03 m^2
Velocity	Y	250 m/s
Deployment Angle	Y	90 degrees
Turbulence Model	Y	SST k-omega
Iterations	Y	250

Table 4.3.7 Setup variables for Ansys Fluent

The variables in Ansys fluent were matched as closely to Autodesk variables as possible, because the primary goal of fluent sims was to validate results from Autodesk CFD. However, it is important to note that for Fluent, a normal surface area was roughly extracted from an analysis of the CAD model, since Fluent requires adjustments to the reference values to obtain sensible numerical results for certain quantities. These

reference values affect only coefficients, in this case the coefficient of drag, but not results for calculated forces. As such, the drag coefficients are not the most robust comparative data between the two by matter of setup. However, the comparative analysis is primarily predicated on the drag force, so this presents little to no issue and may be easily adjusted in the future by editing the simulation's reference surface area.

Another simulation consideration with Ansys Fluent was the way the mesh for the simulation was modeled. In particular, it is relevant to note that a CAD model was imported into Ansys SpaceClaim, where an enclosure was created around it. The CAD model was then suppressed from the whole SpaceClaim, leaving behind an enclosure with a cavity. This enclosure represented a fluid domain, and the approach was deemed appropriate for a preliminary ACS design check, since it was desirable that the flow characteristics be isolated, and no heat transfer between the fluid and solid domains was to be considered.

Convergence:
The Ansys Fluent simulations for both ACS designs were run for a total of **250 iterations**. Initially, the simulations were set to run for 150 iterations; however, this was increased in an attempt to achieve a more refined convergence pattern. Ideally, convergence is represented by a flat line when plotting the numerical results against the simulation iterations. While the increase to 250 iterations did not result in perfect convergence, the results for both the **drag force** and **coefficient of drag** appeared largely stable. It is expected that extending the number of iterations further could result in a narrower range of values, thus improving convergence stability.

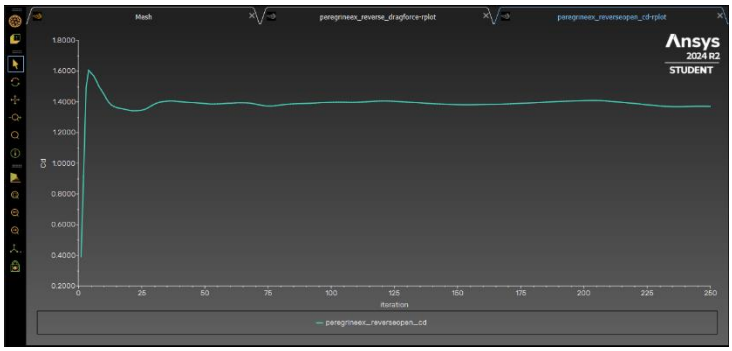

Figure 4.3.11 Coefficient of Drag for Rear-Opening Design

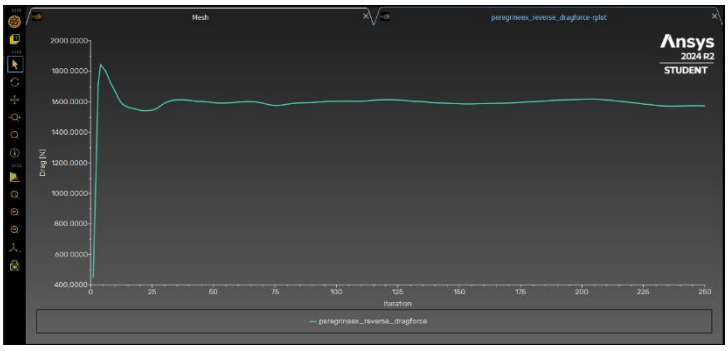

Figure 4.3.12 Drag Force in the Z-Direction Convergence for Rear-Opening Design

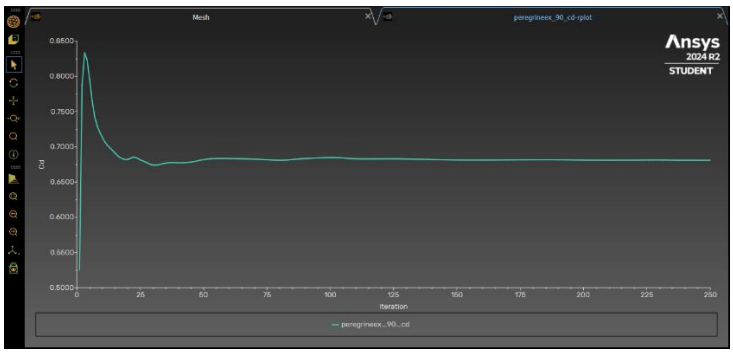

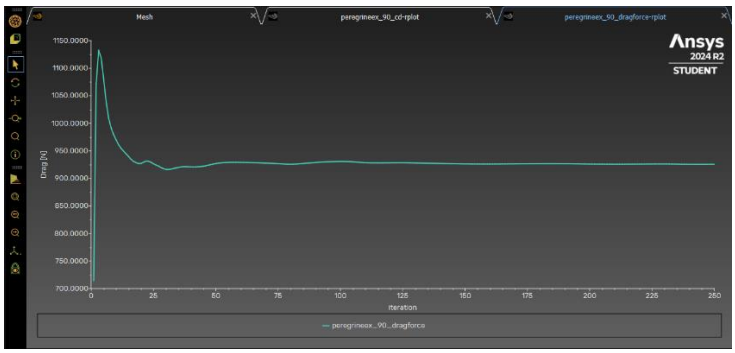

Figure 4.3.13 Coefficient of Drag for Forward-Opening Design

Figure 4.3.14 Drag Force in the Z-Direction Convergence for Forward-Opening Design

Of particular interest in the convergence plots is that the forward-opening design exhibits a more stable convergence in both the drag force and drag coefficient graphs compared to the rear-opening design. This suggests that the rear-opening configuration poses a more complex mathematical problem for the solver. For future CFD simulations, it may be beneficial to set a higher baseline iteration count to achieve more consistent convergence for the rear-opening design. An alternative approach would involve defining specific convergence criteria, such as limiting the numerical force deviation between iterations. This would allow the simulation to determine the optimal point of convergence automatically, leading to more accurate results. If the same convergence criteria were used to achieve convergence on multiple future designs, setting equivalent numerical criteria would be an effective way to maintain consistency between the simulations, thus ensuring a proper, and likely more accurate, comparative analysis.

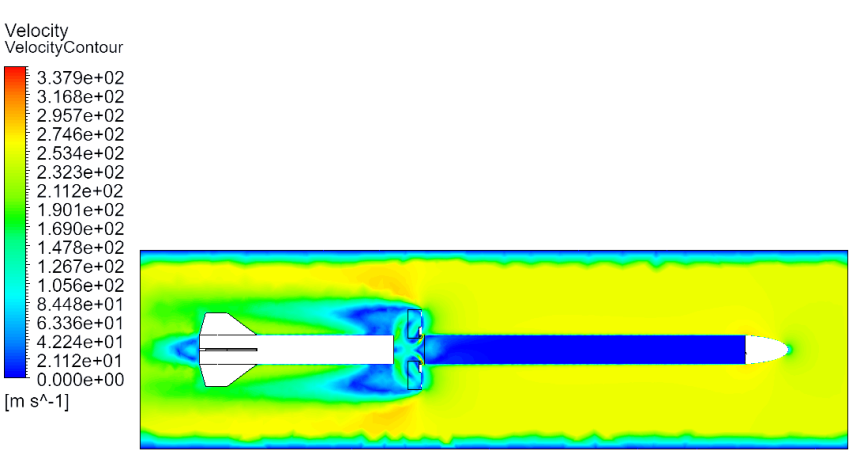

Figure 4.3.15 Ansys Fluent Forward-Opening ACS Velocity Contour

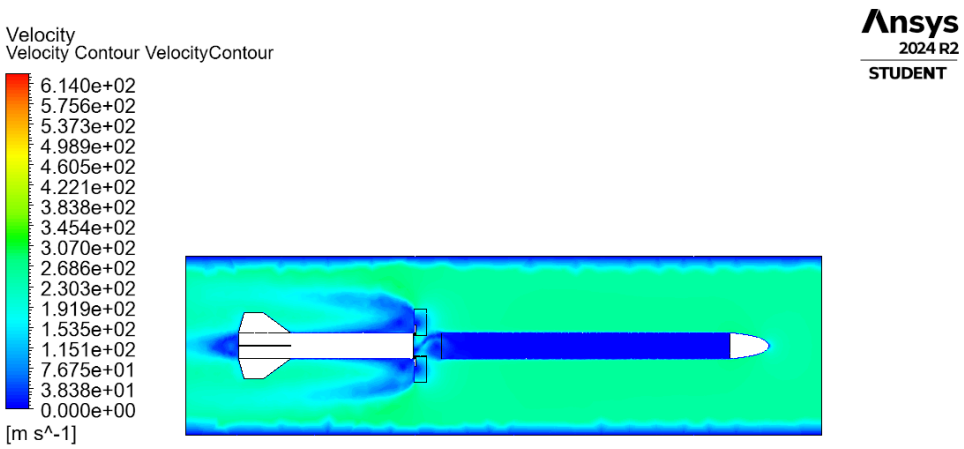

Figure 4.3.16 Ansys Fluent Rear-Opening ACS Velocity Contour

Results:

Quantity	Forward Opening	Rear Opening
Drag Force (N)	925.73395	1573.8998
Coefficient of Drag	0.68095917	1.3704705

Table 4.3.8 Results from Ansys Fluent

The values above indicate that the results from Fluent align with those from Autodesk CFD. CFD platforms determined that the reverse-opening ACS generates more drag compared to the forward-opening design, making it more effective at decelerating the vehicle. The simulations were consistent with an average deviation of 4.9% from the mean, which validates the accuracy of the Autodesk simulations.

Additionally, the velocity contour plots generated by Fluent seem to show similar trends to the CFD Ultimate velocity contour plots. However, the much more extreme velocities reached on the legend of the rear-opening contour plot hint at the potential for greater mechanical loading on this ACS design. As such, the mechanical loading and structural stability must be investigated, with a primary step being finite element analysis to roughly approximate a factor of safety for the design. The greater velocity achieved in the rear-opening design must be considered when deciding which direction to pursue in the design of the altitude control system.

4.3.3.4.3 Cumulative Aerodynamic Analysis Review

The results of the ANSYS Fluent and Autodesk CFD simulations demonstrate a surprising outcome. Despite initial predictions that the rear-opening ACS would perform worse due to the anticipated formation of a turbulent air pocket within the rocket body, the rear-opening ACS design, in reality, exhibited better overall performance. Under identical simulation conditions, the rear-opening ACS generated a drag force that was approximately **648 N** greater than that of the forward-opening ACS.

These findings suggest that the forward-opening ACS design may suffer from vortices generated behind its flaps, leading to air cushioning that impedes airflow over the vehicle's body and potentially reduces drag force. Additionally, the maximum air speed in the rear-opening simulation was observed to be approximately **276 m/s** higher than in the forward-opening simulation, as indicated by the velocity contour plots. This increase in air speed could lead to higher structural loads, raising concerns regarding structural stability and warranting further analysis.

Although these results favor the rear-opening ACS configuration in terms of drag force, the increased structural loads on the system necessitate further investigation. Future simulations should continue to focus on refining drag models and understanding the

underlying aerodynamic phenomena that differentiate these two designs. This will help in optimizing the design for both performance and safety.

The consistency between the CFD software packages validates the results obtained from Autodesk CFD. The data from these simulations were subsequently used to conduct the kinematic analysis of the overall vehicle's performance with the ACS. To develop a method to assess the performance of the ACS, the rear-opening design will be used as a reference model against which future iterations will be compared.

4.3.4 Selected ACS System Performance Analysis

4.3.4.1 Overview

Analyzing the impact of the induced drag from the Altitude Control System (ACS) on the vehicle's flight trajectory was essential to determine whether the design justified further prototyping and financial investment. This analysis was conducted using a set of kinematic equations that describe the motion of a body based on the individual forces it experiences over discrete time steps.

The team identified that a good reference point for this performance analysis would be the data generated by OpenRocket. Once we had an equation model capable of producing an accurate altitude prediction similar to OpenRocket's, we could be confident that the model was sufficient for our ACS calculations. We then modified the model to include induced drag after motor burnout to obtain a new estimation of the altitude profile when using the ACS system.

OpenRocket Simulation	
Variable	Unit
Time	s
Thrust	N
Drag Force	N
Mass	Kg

Table 4.3.9 Simulated values exported from OpenRocket

Table 4.3.9 shows the relevant data needed to develop a basic model that calculates altitude over time. This data was used in the following manner:

At each discrete time step, the total forces acting on the vehicle were calculated. This includes contributions from thrust, aerodynamic drag, and gravitational forces. The equation used to calculate the total force is as follows:

$$F_{Total}\,(t) = Thrust(t) - F_d(t) - Mass\,(t) \cdot g$$

- $F_{Total}\,(t)$: The total forces in Newtons at time t
- $T_{Thrust}(t)$: The thrust(N) provided by the rocket motor at time t
- $F_d(t)$: The aerodynamic drag(N) acting on the rocket, which is a function of velocity and surface at time t
- $Mass(t)$: The mass(kg) of the rocket at time t , which decreases over time due to fuel consumption.
- g : The acceleration due to gravity (assumed constant at 9.81 m/s²).

The total force at each time-step is essential for determining the rocket's dynamic behavior and the subsequent calculations of acceleration, velocity, and displacement.

Once the total forces acting on the rocket were known, the instantaneous acceleration was calculated at each time step using Newton's second law of motion:

$$a(t) = \frac{F_{Total}\,(t)}{Mass\,(t)}$$

Equation: Acceleration

- $a(t)$: Acceleration at time t
- $F_{Total}(t)$: Total forces in Newtons at time t
- $Mass(t)$: Mass(kg) at time t

This step provides the time-resolved acceleration profile of the rocket, which is critical for predicting changes in velocity and altitude.

The next step involves determining the rocket's velocity over time. This is achieved by integrating the acceleration profile, where the initial velocity is assumed to be zero at launch. The velocity at any time

$$v\,(t) = v_0 + \int_0^t a(t)\ \cdot \triangle\, t$$

Equation: Velocity

In practice, the velocity is approximated for discrete time steps using the following iterative formula:

$$v(t) = v(t-1) + a(t) \cdot \Delta t$$

Equation: Discrete Velocity

- $v(t)$**:** The velocity at time t
- $v(t-1)$: Initial Velocity is assumed to be 0 and starts at timestep #2
- $a(t)$: The acceleration at time t
- $\triangle\, t$: The difference in time between current step t and last step $(t\ -1)$

This step provides a time-dependent velocity profile, which is used to further calculate the rocket's displacement (altitude).

Finally, the instantaneous displacement, which represents the rocket's altitude, is obtained by integrating the velocity over time. The displacement at time t , given that the initial altitude is zero at launch, is calculated as:

$$s(t) = s_0 + \int_0^t v(t) \cdot \Delta t$$

Equation: Displacement

In discrete form, this is approximated by:

$$s(t) = s(t-1) + v(t) \cdot \Delta t$$

Equation: Discrete Displacement

- $s(t)$: Displacement at time t
- $s(t-1)$: Initially starts at 0 and timestep #2
- $v(t)$: Velocity at time$t$
- $\triangle\, t$: Difference between current timestep t and previous timestep $(t-1)$

Once applied, a set of altitude values were generated and then charted:

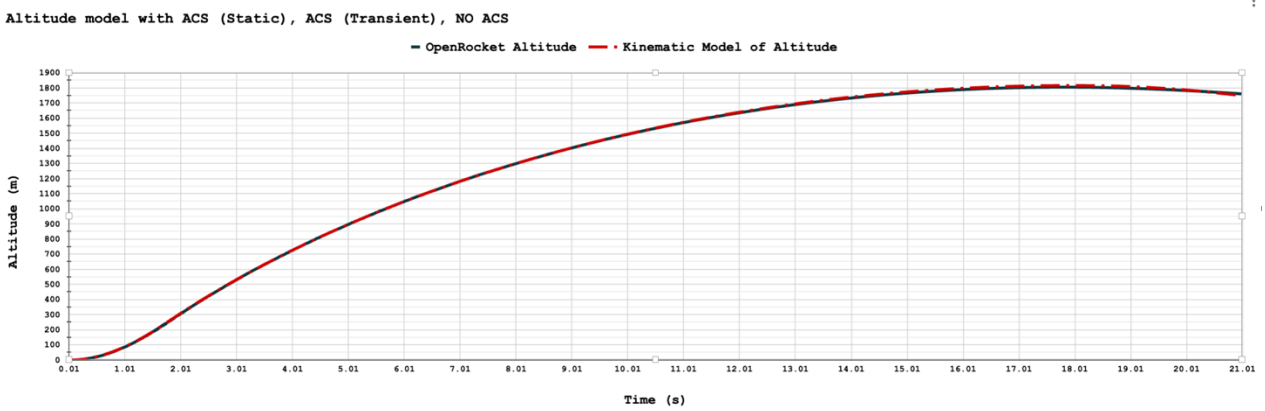

Figure 4.3.17 Calculated altitude using forces on vehicle vs OpenRocket Simulated Altitude

Figure 4.3.17 illustrates that the application of the kinematic equations yields an accurate representation of the rocket's altitude throughout the flight, with minimal deviations from the expected results provided by OpenRocket's reliable simulations. This confirms the accuracy and functionality of our simulation model, allowing for further modification by introducing the drag effects from the ACS deployment.

With the nominal altitude established, the model was modified to include the drag induced by the ACS deployment, providing a projection of the new altitude and apogee under the influence of the aerodynamic braking system.

At each specific time step in the simulation (performed in Excel or similar tools), the total drag force acting on the rocket was adjusted to include the additional braking force generated by the ACS. This additional drag force, acting in opposition to the rocket's motion, was calculated using the drag force equation:

$$F_{BrakingTotal}(t) = F_{Total}(t) - \left(\frac{1}{2} \cdot \rho \cdot A \cdot C_d \cdot v^2(t)\right)$$

$F_{BrakingTotal}(t)$: Total forces under braking at time t

$F_{Total}(t)$: Total forces of just body without ACS deployed

ρ : Air density assumed constant

A : Surface area of vehicle

C_d: coeff of drag of rocket with ACS deployed

$v^2\ (t)$: Velocity at time t

It is important to note that this calculation does not fully capture the behavior of the rocket during the transient deployment phase of the ACS, when the aerodynamic surfaces are transitioning between deployment angles. During this phase, the drag force changes dynamically as the flaps move, and a static $C_d$does not accurately represent the varying aerodynamic characteristics.

To address this limitation in our model, a dynamic drag coefficient chart needed to be established. For this, a series of CFD simulations were conducted, varying both airspeeds and flap deflection angles. The varying air speeds were included to account for convergence noise in the coefficients. The varying deflection angles allowed us to model the dynamic changes in C_d during the deployment of the ACS, capturing how the drag force evolves as the flaps move through different positions.

The result of these extensive simulations and analyses was a comprehensive gradient of drag coefficients across varying deployment angles. This gradient provides a more accurate representation of the drag forces acting on the rocket during the ACS deployment phase, allowing for a precise prediction of the vehicle's trajectory under the influence of the aerodynamic braking system.

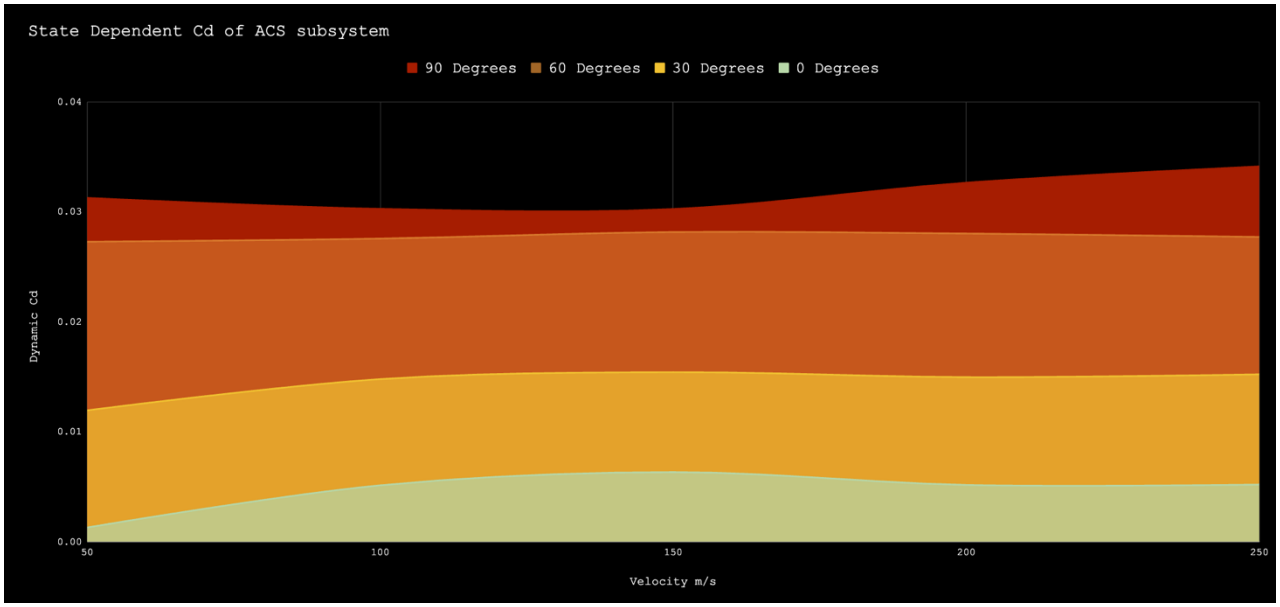

Figure 4.3.18 State dependent C_d of ACS

This chart is key to developing a better analysis model. It illustrates the C_d for each deployment angle of the ACS flaps, ranging from 0 degrees to 90 degrees. By tabulating these C_d values and averaging them across various velocities obtained a more accurate and reliable set of C_d values that reflect the aerodynamic characteristics of the ACS at different deployment angles, independent of the vehicle's speed and variance noise.

				Coeff Drag	
	Speeds m/s				
angles deg	250	200	150	100	50
90	0.02893095765	0.02748497793	0.02392605601	0.02514129764	0.02613558625
60	0.02252205737	0.02286863797	0.02184278464	0.02244251428	0.02215843182
30	0.01002242916	0.009800844844	0.009090638696	0.009658803615	0.006817979022
0	0.005181664057	0.005148994574	0.006312943539	0.005113484267	0.001278371067

Table 4.3.10 Cd matrix through speed and angles

This matrix contains drag coefficients (C_d) computed at various vehicle velocities and ACS deflection angles, derived from Computational Fluid Dynamics (CFD) simulations.

			Drag Force		
	Speeds m/s				
angles deg	250	200	150	100	50
90	1273	774	379	177	46
60	991	644	346	158	39
30	441	276	144	68	12
0	228	145	100	36	9

Table 4.3.11 Drag force matrix through speed and angles

This table provides the corresponding drag forces (F_d) calculated from the drag coefficients for different velocities and ACS deflection angles. After developing a matrix of drag coefficients across a range of speeds and deflection angles, an average of the coefficients across all speed ranges was computed for each deflection angle. This average provided a governing drag coefficient for each specific deflection angle, independent of speed. This process resulted in a set of drag coefficients that describe the behavior of the ACS as it transitions through various deflection angles during deployment.

The table below shows the calculated drag coefficients as the ACS progresses from a fully closed state to a fully deployed state over time:

Time	Cd
0	0.004607091501
1	0.009078139068
2	0.02236688522
3	0.0263237751

Table 4.3.12 Increasing Drag coefficient as ACS fully deploys

This data represents the progression of the drag coefficient as the ACS flaps are deployed, allowing for a dynamic model of the system's drag generation capabilities during deployment. To provide a continuous model of the ACS's drag characteristics, the increasing drag coefficient data was fitted with a third-degree polynomial. This polynomial allows for the accurate calculation of the drag coefficient as a function of time during deployment:

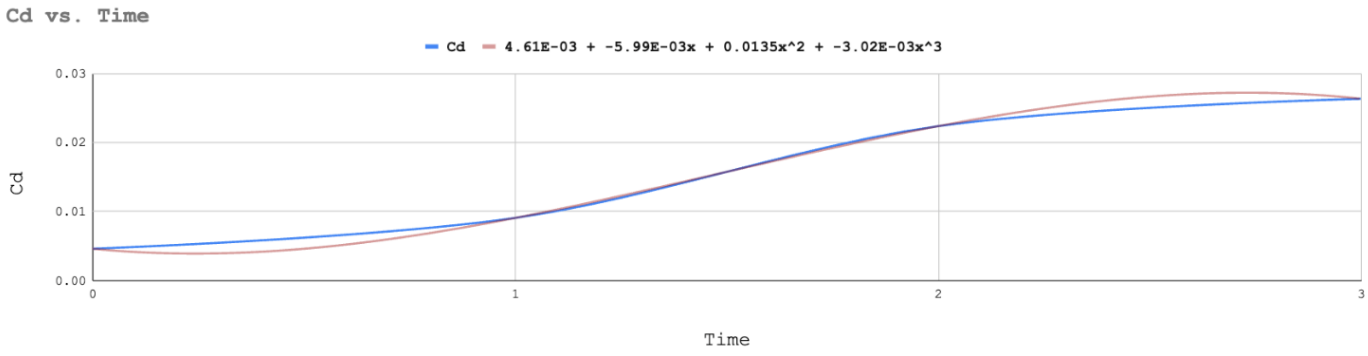

Figure 4.3.18 Polynomial fitted Cd over time as ACS opens

$$C_d(t) = -0.00302t^3 + 0.0135t^2 - 0.00599t + 0.00461$$

- $C_d(t)$: represents the drag coefficient at time t
- The coefficients in the polynomial were obtained through curve fitting, using the calculated C_d values from the CFD data at various deployment angles

This polynomial provides a realistic model of the drag coefficient as the ACS transitions from stowed to fully deployed, offering an accurate representation of the system's behavior over time.Using the drag coefficient polynomial, it is possible to integrate the time-dependent C_d values into the force calculations, allowing for the modeling of the braking force applied by the ACS during its deployment phase. This ensures that the changes in drag during ACS deployment are accurately reflected in the performance model.

The time interval for ACS deployment ($\triangle t_{deployed}$) is calculated as such:

$$\triangle t_{deployed} = Current\ Time\ (t) - ACS\ deployment\ (t_0)$$

To account for the ACS-induced drag during deployment, the total braking force is computed as follows:

$$F_{BrakingTotal}\ (t) = F_{Total}(t) - \left(\frac{1}{2} \cdot \rho \cdot A \cdot \left(C_d\left(\triangle t_{deployed}\right)\right) \cdot v^2(t)\right)$$

$F_{BrakingTotal}$: Total forces under braking at time

$F_{Total}(t)$: Total forces of just body without ACS deployed a time t

ρ : Air density assumed constant

A : Surface area of vehicle assumed constant

$C_d(\triangle t_d)$: Transient C_d model as the ACS opens ($\triangle t_d$ input ranges 0 to 3 seconds)

v : Velocity at time t

By integrating the changing drag coefficients over time as the ACS transitions through deployment, a more accurate, but still idealistic model of the vehicle's performance is achieved.

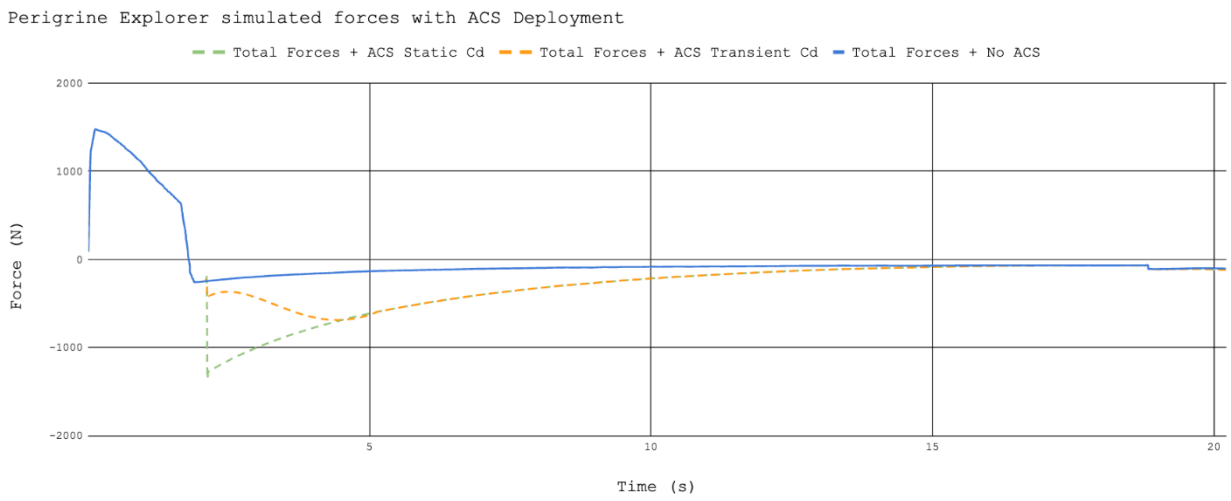

Figure 4.3.19 Simulated Force Profile of vehicle under ACS, No ACS and Theoretically Perfect ACS

The chart above shows how the ACS model with transient C_d doesn't peak in braking force until it is fully deployed.

This refined model increases confidence in the predicted performance of the ACS and provides a more robust framework for assessing the braking efficiency of the system.

4.3.4.2 Results

With the cumulative total forces resulting from the ACS deployment now calculated, the next step is to evaluate the altitude trajectories for the different ACS models. This assessment was performed using the equations for Acceleration, Discrete Velocity, and Discrete Displacement, allowing for a detailed comparison of the rocket's flight path under different conditions.

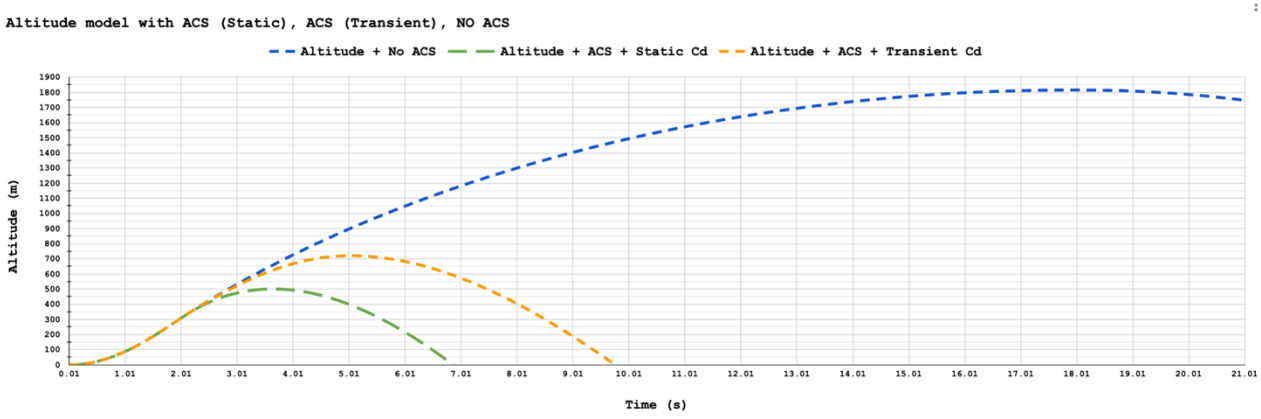

Figure 4.3.20 Altitude model of vehicle utilizing ACS after motor burnout

The results of the simulations are summarized in Figure 4.3.20. The figure illustrates the maximum apogee achieved by the vehicle under the following conditions:

- Without ACS**:** The vehicle reaches a maximum apogee of approximately 1814 meters (5951 feet) in the absence of the ACS, demonstrating the unrestrained flight profile.

- Instant ACS Deployment: In a scenario where the ACS is assumed to deploy instantly at its maximum drag configuration, the maximum apogee is drastically reduced to 500 meters (1640 feet). This serves as a theoretical lower bound for altitude reduction.

- Realistic ACS Model (Time-Dependent Drag Coefficient): In a more realistic model where the drag coefficient transitions gradually during ACS deployment, the maximum apogee is measured at 720 meters (2362 feet).

This yields a total reduction in altitude of approximately 1094 meters (3589 feet) when compared to the unrestrained flight without the ACS. Clearly demonstrating

the substantial impact of the ACS on the vehicle's altitude trajectory. The instant deployment model serves as an idealized scenario, where maximum drag is applied immediately upon deployment. This represents a theoretical lower bound for altitude. In contrast, the realistic deployment model, which incorporates a time-dependent drag coefficient, offers a more accurate reflection of the system's behavior in real-world conditions, accounting for transient effects during ACS deployment.

Given these results, the ACS design concept is approved for further development, as it effectively reduces the vehicle's apogee and meets the intended design objectives. However, it is recommended that the design undergo further optimization to better balance the safety factors and the braking potential of the system. This is especially important due to the substantial forces experienced by the subsystem at near-transonic velocities. Additional considerations should be given to ensuring structural integrity and reliability under these high aerodynamic loads.

Future optimization efforts should focus on refining the ACS deployment mechanism to mitigate excessive stress during deployment, while maintaining the desired braking effect. The results indicate that with further adjustments, the ACS can provide reliable altitude control while minimizing risk.

4.3.5 ACS Subsystem Safety

The Altitude Control System (ACS) is not a required component of the launch vehicle as per the competition guidelines, making its functionality secondary to the primary systems and the overall safety of the vehicle. In the event of an ACS failure during flight, the system is designed to prioritize vehicle safety. This may involve refraining from deploying the airbrakes, even when needed to achieve the desired apogee, or retracting the airbrakes to prevent any adverse impact on the vehicle's aerodynamics.

Safety considerations will be integrated into both the mechanical and software design phases to address all potential failure modes. To mitigate the risk of mechanical failure, each flap will be supported by linkages connected to a primary rod made of Aircraft Grade Aluminum 6160. These linkages will interface with the primary lead screw for control. This design not only minimizes wear on the lead screw but also introduces possibility of incorporating springs into the system to store potential energy. These springs could assist in faster deployment, improving performance by releasing energy during actuation. Alternatively, the springs could be configured in a reverse

manner to add safety by automatically closing the ACS in the event of a system failure. In the forward configuration, which is the likely design due to inherent safety concerns, the ACS will passively close when not under power, as aerodynamic forces will push the flaps closed. These mechanical fail-safes will activate in case of any issue, allowing the vehicle to maintain stability and coast to apogee without the ACS.

On the software side, the system will leverage the onboard Inertial Measurement Unit (IMU) to assess the vehicle's angular velocity and detect any flight anomalies. The IMU will ensure that the ACS remains inactive during the motor burn phase and will provide real-time measurements of angular velocity and acceleration along the rocket's primary axes. A safety protocol will be implemented to monitor these parameters, and if a significant deviation from nominal flight conditions is detected—beyond a predefined threshold—the ACS will not deploy.

In addition, if any unexpected disturbances, such as an induced tumble, are encountered during the coast phase resulting from ACS activation, the system will automatically shut down to prevent further instability. The exact threshold values for detecting perturbations along the vehicle's pitch and yaw axes will be determined after analyzing the vehicle's dynamic behavior. These thresholds will be set based on angular velocities that could lead to instability. While some rotational movement along the roll axis is expected during normal flight, the thresholds for pitch and yaw will be specifically tuned to prevent the ACS from negatively impacting vehicle orientation during coast.

Comprehensive testing will be conducted to validate the system's performance. This will include simulations, mechanical testing up to failure loads, and real-world vehicle demonstration tests. The integration of data-driven design alongside rigorous testing will ensure the smooth, safe operation of the ACS and maximize competition points through optimized performance.

5 Safety

The safety of the operation is paramount to our success, as any failure can delay the team enough to miss a deadline or be expensive enough to require extra funding to recover. It also ensures that all equipment, surrounding environment, properties, and people in and around the launch area are safe and are not at risk of being damaged or harmed. Knowing the dangers helps keep everyone and anything safe as steps can be made to avoid incidents.

5.1 Hazard Analysis Methods

Hazard analysis is based on two factors: Likelihood and severity. Likelihood is the rarity of which events occur and severity is what impact(s) an event will cause.

5.1.1 Failure Occurrence Likelihood

Level	Category	Definition
0	Rare	Failure mode is Extremely Unlikely to happen
1	Unlikely	Failure mode is unlikely to occur
2	Plausible	Failure mode has average odds to occur
3	Likely	Failure mode is likely to occur
4	Common	Failure Mode has happened before and/or is very likely to happen

Table 5.1: Risk Likelihood Table

5.1.2 Failure Effect Severity

Level	Category	Health and Safety	Equipment	Environment	Project
A	Negligible	No First aid required	Cosmetic Damage	No risk or damage to environment	No impact to Project timeline or goals
B	Minor	First aid was provided. Less than 1 day recovery time.	Damage is noted but can continue to operate with little to no detriment to the machine.	Slight damage to the environment, no clean up or action needed	Less than 1 day delay, no long-term impact
C	Moderate	First Aid Provided. Gause or other large bandage, Recovery time over 1 day	Reversible machine failure, requiring near-immediate repairs.	Damage to the environment that requires team intervention, but no long-term effects or reporting needed.	Delay of up to 1 week, may impact testing / flight schedule, no effect of deadlines
D	Major	Serious Injury requiring	Total machine failure	Severe damage to the	Delay of over 1 week,

		hospitalization, no long-term effects.	requiring repairs before continuing usage	environment, immediate team intervention required, reporting to relevant agency	testing/ test flights will slip. Risk of missing deadline
F	Catastrophic	Life Threatening injury or serious injury that results in long-term injury/disability	Total irreversible failure of equipment requiring replacement	Extreme damage to the environment requiring immediate government intervention	Delay of over 1-month, high risk of missing deadline, retirement from competition.

Table 5.2: Failure Effect Table

5.1.3 Risk Analysis

The table below uses the likelihood analysis and Severity analysis to create a Risk Hazard Matrix. The Matrix is then color-coded into the following Categories.

- Green: Marginal
- Yellow: Slight
- Orange: Enhanced
- Red: Moderate
- Magenta: High

		Severity				
		A - Negligible	B - Minor	C – Moderate	D – Major	F - Catastrophic
Likelihood	1 – Rare	1A	1B	1C	1D	1F
	2 – Unlikely	2A	2B	2C	2D	2F
	3 – Possible	3A	3B	3C	3D	3F
	4 – Likely	4A	4B	4C	4D	4F
	5 – Very Likely	5A	5B	5C	5D	5F

Table 5.3: Risk Analysis Matrix

5.2 Personnel Hazards Analysis

Hazard	Likelihood	Severity	Risk	Mitigation	Verification	Post Mitigation Risk
Entanglement with machinery	1 (Working with manual machines)	F (Loss of body part, severe injury, required hospitalization	1F, Enhanced	Members only allowed to use machinery are trained properly, use of buddy system in labs	Call out before use to make sure members are informed of hazards. Oversight by team officers	1D, Slight
Contact with falling equipment	1 (Dropped items or falling items)	C (Injuries including bruising, cuts, hospitalization in worst case scenario)	1C, Slight	Secure items that are heavy to worktables, use carts to transport heavy/bulky items	Call out before use to make sure team members are informed about hazards. Oversight by team officers	1C, Slight
Fire in workshop	2 (Damage to LiPo batteries, sparking equipment, epoxy, overheating, improper disposal of wash rags)	F (Loss of workspace, severe burns to personal)	2F, Moderate	Know where fire prevention equipment is stored, store hazardous material in proper containers	Make sure all members are informed on fire safety protocol	1F, Enhanced
Contact with airborne chemical/debris	3 (Airbourneparticles made during manufacturing process)	B (Minor abrasions/burns)	3B, Slight	Wear proper PPE. Including; gloves, eye protection, lab coat, rinse with water if come into contact	Safety team subsystem leads, will enforce PPE usage, safety procedures	1B, Marginal

Contact with hazardous chemicals	3 (Chemical spills, improper chemical usage)	C (Burns, abrasions)	3C, Enhanced	Wearing appropriate PPE; Gloves, lab coat, and eyewear. Wash with water. Dispose in proper container	Call out before use to make sure team members are informed about hazards. Oversight by team officers	1C, Slight
Dust/Chemical Inhalation	3 (Particle debris)	C (Short-term respiratory damage)	3C, Enhanced	Wearing appropriate PPE; N95, eyewear, lab coat (optional). Working in well-ventilated area. Wash with water	Call out before use to make sure team members are informed about hazards. Oversight by team officers	1C, Slight
Electrocution	3 (Work with custom PCBs, LiPo batteries)	C (Short-term nerve damage, electrical burns)	3C, Enhanced	Ensure team is working with proper PPE, treating all electronic circuitry as if it is live	Oversight by team officers	2C, Slight
Epoxy Contact	3 (Assembling components on vehicle, small repairs, fabricating test samples)	B (Skin Irritation)	3B, Slight	Wear appropriate PPE; gloves, N95, glasses optional	Call out before use to make sure team members are informed about hazards	1B, Marginal
Eye Irriration	3 (Airborne debris, smoke)	B (Temporary eye irritation)	3B, Slight	Wear proper PPE. This includes protective eyewear and wash eyes if contact made	Call out before use to make sure team members are informed about hazards	1C, Slight
Contact with heat sources	3 (Working with epoxy or sharp tools)	B (Slight burn/skin irritation)	3B, Slight	Ensure that members are wearing the proper	Call out before use to make sure team members are	1B, Marginal

				PPE, letting items cool after working them	informed about hazards	
Power tool cuts, lacerations, and injuries	3 (Cuts from drill bits, rotary tools, exact-o blades/box cutters	D (Lacerations, avulsions, hospitalization, plausible)	3D, Moderate	Secure hair, clothing, jewelry, wear proper shoes. Appropriate PPE	Call out before use to make sure team members are informed about hazards	1D, Slight
Tripping Hazards	3 (Equipment not put away, wires on ground)	C (Upper body injuries, bruising from walking into objects)	3C, Enhanced	Brief team on picking up equipment in hazardous way	Enforce cleaning procedure	1C, Slight
Dehydration/Heat exhaustion	4 (Hot sunny days, working in hot labs)	B (Fatigue or passing out risk)	4B, Slight	Reminding members to drink water and wear breathable clothes, if signs of dehydration or heat exhaustion are present, members must be forced to take break and drink water	Oversight by officers	3B, Slight
Hearing Damage	4 (Proximity of loud or high-pitched noise)	D (Long term hearing damage)	4D, Moderate	Ensure team is wearing hearing protection if around loud/high-pitched for longer than 10 minutes	Call out before use to make sure team members are informed about hazards	1D, Slight

5.3 Failure Mode and Effect Analysis

Hazard	Likelihood	Severity	Risk	Mitigation	Verification	Post Mitigation Risk
Onboard Vehicle Fire	1 (Electric fire/fire spread due to motor failure)	F (Falling debris, unaccounted for vehicle separation, ground/brush fire)	1F, Enhanced	To reduce or prevent fire spread, install “fire compartments," separating critical hardware from each other.	Cover exposed wires with insulators and install heat insulators if needed.	1F, Enhanced
Fastener Failure	2 (Excessive force)	F (Irreversible damage to vehicle, falling debris, dangerous flight path to people and surroundings)	2F, Moderate	Increase number of simulations and increase safety factor of flight critical components to 2+	Physical testing to confirm manufacturer specifications	1F, Enhanced
Thrust Structure Failure	2 (Poor construction, motor overperformance causing excessive force)	F (Irreversible damage to vehicle, falling debris)	2F, Moderate	Increase number of simulations and increase safety factor of flight critical components to 2+	Physical testing of motor mount assembly to 200% the expected force of boost	1F, Enhanced
Recovery System Failure: Drogue Stage	2 (Bad product control on ejections charge ignitors, airframe shoulders having high friction, drogue	F (failure to prevent ballistic trajectory, high energy non-ballistic descent)	2F, Moderate	Implement checks for ignitors to ensure continuity, size primary and backup ejection charges to be at least 130% the required force to deploy the system, ensure both parachute and	Ground testing and maintenance of the airframe to prevent binding	1D, Slight

	parachute failure)			protector are intact before use		
Structural Failure of Bulkheads	2 (Poor construction, faulty modeling/simulation)	F (Falling debris)	2F, Moderate	Design components to a safety factor of 2	Testing of bulkheads to validate computer modeling	1F, Enhanced
Damaged Nose Cone, Payload Compartment	2 (Poor, Construction, Flight/transportation damage)	D (instability, Damage to payload, Dangerous flight path to personal and surroundings)	2D, Enhanced	Ensure that the descent rate of section is below damaging levels, provide protective packing when transporting	Inspect material between launches	1C, Slight
Component Misalignment: Motor mount tube/assembly	2 (Poor construction, bad manufacturing plan, bad product control of construction components	D (Launch vehicle does not follow flight path, severe instability)	2D, Enhanced	Use tools from CNC lab to measure all components to verify eccentricity and location	Have multiple engineers verify measurements	1D, Slight
Commercial Rocket Motor Failure	2 (Faulty motor preparation, defect from manufacturer)	F (Destruction of vehicle section, Falling debris)	2F, Moderate	Purchase propellant from reliable sources, only team mentor is allowed to handle and assemble the motor	Safety officer will observe preparation and integration	1F, Enhanced
Recovery System Failure: Tether, Riser, or Shock Cord Failure	3 (Excessive force, Burn through from the ejection	F (Falling debris, high-energy non ballistic landing)	3F, Moderate	Use higher quality materials, fire resistant materials/coverings, use tethers that are	Ground testing and inspections between flights and testing. During assembly, multiple	1F, Enhanced

	charge deployment)			200% the strength of the expected loading	engineers verify that connections are torqued to spec	
Recovery and Tracking Avionics Power Failure	3 (Faulty wiring, design not resistant to flight forces)	F (Recovery device may not deploy, Ballistic landing)	3F, Moderate	Testing avionics bay assembly to investigate reaction to flight forces, observe set up before and after test flights to validate data	Continuity and “pull tests” will be performed during avionics bay integration to test wire connectivity and attachment	1F, Enhanced
Recovery System Failure: Main Stage	4 (Bad product control on ejection charge ignitors, airframe shoulders having high friction, Main parachute failure, failure to fully deploy from parachute bay	D (High energy non-ballistic landing)	4D, Moderate	Implement checks for ignitors to ensure continuity, size primary and backup ejection charges to be at least 130% the required force to deploy the system, ensure both parachute and protector are intact before use	Ground testing and maintenance of the airframe prevent binding	1D, Slight
Altitude Control System Mechanical Failure	3 (material failure of the ball screw, linkages, or aerobraking surfaces)	F (leaving vehicle in unknown aerodynamic state, Dynamic Instability, unsymmetrical deployment leading to high AOA at high velocity)	3F, Moderate	Ensuring all mechanical parts of a safety factor of 3+.	Extensive ground testing: wind tunnel testing, simulated load testing. Asymmetric deployment studies.	2F, Enhanced

Altitude Control System Electrical Failure	3 (custom PCB being manufactured wrong causing electrical fault)	D (fire, fatal damage to component leading to ACS staying in the same deployment state)	3D, Moderate	Increased electrical design studies are needed to ensure the PCB design is sound.	Ground testing including testing a sacrificial board to failure to find true limits of system	1C, Slight

5.4 Environmental Concerns

Hazard	Likelihood	Severity	Risk	Mitigation	Verification	Post Mitigation Risk
Collisions with Structures	3 (Structures are near minimum clearance for High-Power at Amesbury (1500ft))	D (Damaging Roof, landing on hard surface damaging vehicle)	3D, Slight	Aiming rocket away from structures. Weather forecasting winds at the surface and at altitudes to visualize wind shear to aid in determining launch direction	Doing simulations with different wind scenarios to find the furthest distance a rocket will drift down/cross range	1D, Slight
Contact with Wildlife	1 (Wildlife interacting with vehicle after landing)	C (Animal interacting with residue from flight or damaging vehicle)	1C, Slight	Install deterrents on the vehicle to scare off wildlife. This includes buzzers.	Safety briefing talking about what hazards may be present, educating members on how to interact with wildlife	1C, Slight
High Temperature	2 (Hot weather in Huntsville, abnormal heat in winter)	C (On-board batteries and support overheating causing damage, heat exhaustion stroke)	2C, Slight	Observing weather forecast and temperatures above 80F classified as hot weather. 90F and above is classified as	Ensure team members are properly prepped for extreme heat. Possibly running a car with AC to provide a	1C, Slight

				extreme heat. Bringing pop-up tents, providing shade for the team and equipment, as well as bringing water for the team.	cooler environment for equipment and team	
Battery Leakage	2 (Battery damage from flight)	D (Fire or chemical residue from combustion of hazardous material)	2D, Enhanced	Protect battery from flight forces and landing forces.	Safety briefing about what hazards may arise or be present, inspect battery between flights for damage	1D, Slight
Fire	2 (Motor failure near ground, on-board fire continuing to landing)	F (Fire on ground, pollution from)	1F, Enhanced	Using ground protector next to the launch pad, bringing fire suppression equipment.	Safety briefing about hazards that may be present	1F, Enhanced
Unstable Ground	2 (Loose rocks/dirt, mud)	B (Personal or equipment falls)	2B, Marginal	Inspect area of launch pad and prep-area for ground hazards	Safety briefing about hazards that may be present	1B, Marginal
Landscape	3 (Trees, streams, rocks)	D (Unable to recover rocket, water damage to components or electronics, physical damage)	3D, Moderate	Scout out launch-field for hazards and aim away, use forecast to determine wind to help aid aim	Inspect launch site pre-launch to verify mitigation	2C, Slight
Visibility	3 (Exceeding operating limitations of 14 CFR 101.25)	D (Scrubbing launch, delay of 1 day to 1 week)	3D, Moderate	Weather forecasting and scheduling back up at launch windows to allow for	Check weather forecasts and creating a launch weather	1D, Slight

				weather related delays	criteria list to allow a safe launch at range	
Pollution from Vehicle	3 (Debris from vehicle from an in-air failure or damage during landing)	C (Small pieces of debris left from vehicle that pose minimal effect of the environment)	3C, Enhanced	If a failure is noticed, the team forms a “Police Line” and searches the field for debris. Landing site is investigated for debris	Initial inspection of vehicle at landing zone and preparation area to determine if any items have been dislodged or removed	1C, Slight
Pollution from Team	3 (Wrapper from motor reload, trash from vehicle integration, snack-wrappers)	C (Small debris from team)	3C, Enhanced	f a failure is noticed, the team forms a “Police Line” and searches the field for debris. Ground will be searched for any trash	Installing Pack-in/Pack-out mentality in team. “Leaving field better than when arrived”	1B, Marginal
Humidity	4 (Humid climate)	C (Condensation creating electrical shorts, humidity affecting adhesive or materials)	4C, Enhanced	Construction and storage of construction materials and motors in climate-controlled rooms, electronic boards given conformal coating to give them resistance to short across traces	Check forecast	2B, Marginal
Winds	4 (High winds preventing launch, winds blowing in	D (Scrubbing launch, rocket landing outside launch site)	4D, Moderate	Forecast and back-up launch days	Checking forecast and creating a launch weather criteria list to ensure safe launch	1D, Slight

	unsafe direction)					
Rain/Weather	4 (Cannot launch in rain or cloud cover)	D (Scrubbing delay launch, delaying of 1 day to 1 week)	4D, Moderate	Weather forecasting and schedule back up windows in case of weather delays	Checking forecast and creating a launch weather criteria list to ensure safe launch	1D, Slight
Low Temperature	4 (Cold plunge in New England Region with temperatures below 40F)	D (Damage to propellant reload, hypothermia and frostbite, reduced performance of battery)	4D, Moderate	Bring heaters, handwarmers, and insulating equipment under 40F. Activities limited/suspended below 10F	Check forecast. If necessary, suspension of outside activities may be called at any point, provide running car with heat	2D, Enhanced
Pollution from Motor Exhaust	5 (Combustion by products from firing commercial rocket motor)	A (Small quantities of greenhouse gases, hydrochloric acid, NOx/SOx compounds)	5A, Slight	Use NAR/TRA approved rocket motors	Motors used to launch test vehicles and competition flight will be inspected by safety officer to ensure compliance	5A, Slight

5.5 Project Risk Analysis

Hazard	Likelihood	Severity	Risk	Mitigation	Verification	Post Mitigation Risk
Lack of Funding	4 (First Year Attempting NASA USLI, No Current Corporate Sponsorships)	D (Unable to afford Equipment, Unable to Attend Launch in Huntsville)	4D, Moderate	Aggressive Fundraising Campaigns (Crowdsource Campaign and looking for sponsors)	The Business Team Lead will work with the Student Launch Team lead to ensure the club is raising enough money for the competition	3B, Slight

Failure to Receive parts	2 (ordering from unreliable sellers)	C (Multiple day delays from shipping, ordering new parts)	2C, Slight	Order parts from verified sellers and legitimate websites	Verifying links and auditing purchase orders	1C, Slight
Damage or Loss of Parts/gear	3 (improper part care during construction, testing, or launch)	C (cannot construct vehicle or continue testing)	3C, Enhanced	Creation of multiple replacement parts when applicable, owning spare sets of equipment	Extra parts ordered for all needed systems	2C, Slight
Rushed/bad workmanship	3 (Approaching deadlines, unreasonable schedule expectations)	D (Testing failures & launch failures due to low-quality construction)	3D, Moderate	Built-in schedule buffers so deadlines aren't stressing	Pre-flight inspection and following tolerances	2C, Slight
Unavailable Launch Area for Test Flights	3 (Unhappy neighbors, fields not in condition to fly, no-waiver to fly)	F (delay of multiple weeks to get to flight, disqualification from the project due to no subscale & vehicle demonstration flight data)	3F, Moderate	Being in contact with multiple NAR sections near us, like St. Albans, VT CRMRC. Attempting launches early in the period to allow for scheduling issues	The Safety officer will work with team mentor to secure fields for testing at least 45 days in advance.	1F, Enhanced
Testing failure	3 (bad design, unforeseen mechanisms leading to failure, commercial component failure)	D (Damage to vehicle, failure of subscale or vehicle demonstration flight)	3D, Moderate	Following standard practice as set by team's mentor, designing critical systems to be redundant	Safety officer will ensure that all sub-systems are being designed with a proper safety factor and considerations	1D, Slight

Loss of work area	2 (Fire, loss of lab privileges, Closures during school breaks)	F (Inability to construct vehicle)	2F, Moderate	Follow regulations and rules set by team and workspace occupied	Team Officers will ensure that the team will be utilizing each space we occupy correctly and follow the rules set in place by the safety agreement	1D, Slight
Failure in construction equipment	2(Improper maintenance, improper use)	D (Long-term delay in project for replacement)	2D, Enhanced	Ensure members using tools and equipment are trained properly, owning back-up equipment that can be used in the event of a failure	Each member will be responsible for maintaining equipment following the team safety agreement	1D, Slight
Insufficient Transportation	4 (lack of funding or space to bring available members to off-campus testing, launches, or workplaces)	C (Loss of sufficient labor, loss of transfer of knowledge to new members, loss of work efficiency)	4C, Enhanced	Organize and budget for transportation early and plan expenses in advance	Project management and team leads will be responsible for communicating when activities are being held and plan transportation to the events	2C, Slight
Lack of members available to work	4 (shared class deadlines or mid-term exams takes out sections of team)	C (Some classes may require multiple days of studying before an exam)	4C, Enhanced	Work with team members to “forecast” when class work will be high to help schedule time to work on project with the rest of the team	Team leads meetings to verify that members are not being overloaded with school and project work	3C, Enhanced

Lack of Knowledge	5(members new to the club / hobby not understanding what each component does)	B (needing to take a section of the meeting to educate groups of members on standard rocketry practices)	5B, Enhanced	Create a resource of online tutorials for members to look at, and create our own PowerPoint slide decks with similar information	Have set meetings throughout the semester where a team lead will discuss their section of the rocket and what every part does	3B, slight
Bad Communication	5 (Members not knowing what to work on, sub-teams skipping critical tasks)	C (creates confusion in the team and can potentially derail the project or cause a backlog of work during the milestone reports)	5C, Moderate	Make Sub-team meetings more efficient, creating task checklists, opening new operations positions to aide in project management	Oversight by operations team.	2C, Slight

6 Project Plan

6.1 Mission Success Criteria

The ultimate goal of the Peregrine Explorer mission is for the UMLRC to attend and fly at its first ever competitive rocketry event. This will be the minimum requirement for the team to consider the work done on the project, however the fully integrated vehicle also has set mission criteria to be considered a successful flight. The minimum requirements as set in the handbook are listed for each major system below, along with the team-specified mission requirements.

6.1.1 Vehicle Success Criteria

The design of Peregrine Explorer follows all criteria put forward in section two of the USLI Handbook including but not limited to, reusability, number of body sections (4 or less), coupler tubing lengths, motor limitations, and electronic autonomy limitations. The team has developed the vehicle's fin assembly to be interchangeable to maximize the ability to re-fly the vehicle despite any damage. Replacement parts will be available on launch day to quickly change the fins in the event of a structural failure.

6.1.2 Recovery System Success Criteria

The Recovery System has been designed to maximize chances of recovery. Both of the vehicle's flight computers are separately powered and individually trigger their own sets of parachute deployment devices to ensure full redundancy. All sections of the vehicle have been limited to be below 50 ft-lbf of kinetic energy to ensure any damage upon landing is mitigated as much as possible. Main parachute deployment will be set at an altitude at or above 600ft to deploy the parachute as intended and ensure vehicle survival.

6.1.3 Payload Success Criteria

6.1.3.1 PERR-C Success Criteria

PERR-C is designed to transmit all 8 options of flight data as outlined in the USLI handbook. The decision to prioritize all of these over the required 3 is driven by the desire to maximize the amount of data collected from the landing site as much as possible. The sensor suite selected has been selected to accomplish this goal. The primary payload is also designed to be entirely contained inside of the flight capsule for the duration of the mission to minimize payload complexity and ensure mission success.

6.1.3.2 ACS Success Criteria

ACS is Peregrine Explorer's secondary payload with the express purpose of actively narrowing the vehicle's apogee to within 100ft above and below the target altitude. Narrowing this range ensures that the vehicle will be at a predictable altitude for drogue parachute deployment. It also minimizes the time that the vehicle will be in the air. Minimizing the amount of data to process for transmission.

6.2 Budget

6.2.1 Vehicle Bill of Materials

Part	P/N	Q of Parts	Material	Source	Q of Materials	Base Cost	Tax	Total Cost
Nosecone Bottom		1	PLA	Makerspace	N/A	$-	$-	$-
Nosecone top		1	PETG	Makerspace		$-	$-	$-
I-Nut	3274T71	1	Steel	Mcmastercarr			$-	$-
1/4 20 steel threaded rod		1	Steel	Mcmastercarr			$-	$-
5ft body tube	GT12 3.9	4	Fiberglass:GT12 3.9	Wildman			$-	$-
Coupler tube 1in	GT12 3.9	60	Fiberglass:GT12 3.9	Wildman		$2.33	$0.15	148.5375
Fins		4	Polycabonate	Makerspace			$-	$-
2 Meter Radios		1		Amazon		$49.99	$3.12	$53.11
Flight Batteries		1		Amazon		$21.99	$1.37	$23.36
BNO055	4646	1		Adafruit		$29.95	$1.87	$31.82
3S Li-Po’s		1		Amazon		$34.99	$2.19	$37.18
PWM tester		1		Amazon		$8.99	$0.56	$9.55
ACS motor driver	2448	1	18-8 Stainless Steel	Adafruit		$6.95	$0.43	$7.38
McMaster Threaded Stud	97042A176	2	18-8 Stainless Steel	McMastercarr		$8.92	$0.56	$18.96
Heat Shrink Tubing		1		Amazon		$11.99	$0.75	$12.74
Multi-Wire Stripper Tool		1		Amazon		$19.99	$1.25	$21.24
4-40 Square Nuts	94855A281	1	Zinc plated steel	Mcmastercarr		$3.37	$0.21	$3.58
XT30 Connectors		1		Amazon		$11.99	$0.75	$12.74
4-40 Heat Set Inserts		1		Amazon		$10.99	$0.69	$11.68
ESP32-S3 feather	5477	1	Electronics	Adafruit		$17.50	$1.09	$18.59

BMP388	3966	1	Electronics	Adafruit		$9.95	$0.62	$10.57
ADXL375	5374	1	Electronics	Adafruit		$24.95	$1.56	$26.51
ICM-20948 9-DOF Gyroscope	4554	1	Electronics	Adafruit		$14.95	$0.93	$15.88
RFM69HCW Transceiver Radio	3070	1	Electronics	Adafruit		$9.95	$0.62	$10.57
Raspberry Pi Pico 2 - RP2350	6006	1	Electronics	Adafruit		$5.00	$0.31	$5.31
Breadboard	443	2	Electronics	Adafruit		$19.95	$1.25	$42.39
MPL3115A2	1893	1	Electronics	Adafruit		$9.95	$0.62	$10.57
Flash Memory	6038	1	Electronics	Adafruit		$10.95	$0.68	$11.63
GPS Chip	4415	1	Electronics	Adafruit		$29.95	$1.87	$31.82
Jumper Wires		1	Electronics	Amazon		$7.99	$0.50	$8.49
Remove Before Flight Tags x10		1	Cloth	Amazon	N/A	$17.99	$1.12	$19.11
PolyLite™ ASA (1kg)	PF01011	1	PLA	Polymaker	1kg	$31.99	$2.00	$33.99
PolyLite™ PETG (1kg)	PB01015	1	PETG	Polymaker	1kg	$22.99	$1.44	$24.43
PolyLite™ PETG (1kg)	PB01024	1	PETG	Polymaker	1kg	$22.99	$1.44	$24.43
PolyMax™ PC (750g)	PC02004	1	PC	Polymaker	750g	$38.99	$2.44	$41.43
							$-	$-
Total						$518.48	$32.41	$727.62

Table 6.2.1: Vehicle Bill of Materials

6.2.2 Total Planned Expenses

Group	Cost	% total
Vehicle BOM	727.62	6.61
vehicle buffer (+10%)	72.762	0.66
Plane tickets	3100	28.17
rental cars / gas	1400	12.72
Hotels	2500	22.72
engagement	250	2.27
Rocket Motors and Shipping	1520	13.81
Pre Total	9570.382	
Project Buffer (+15%)	1435.557	13.04
Total	11005.94	100.00

Table 6.2.2: Overall Project Projected Expenses

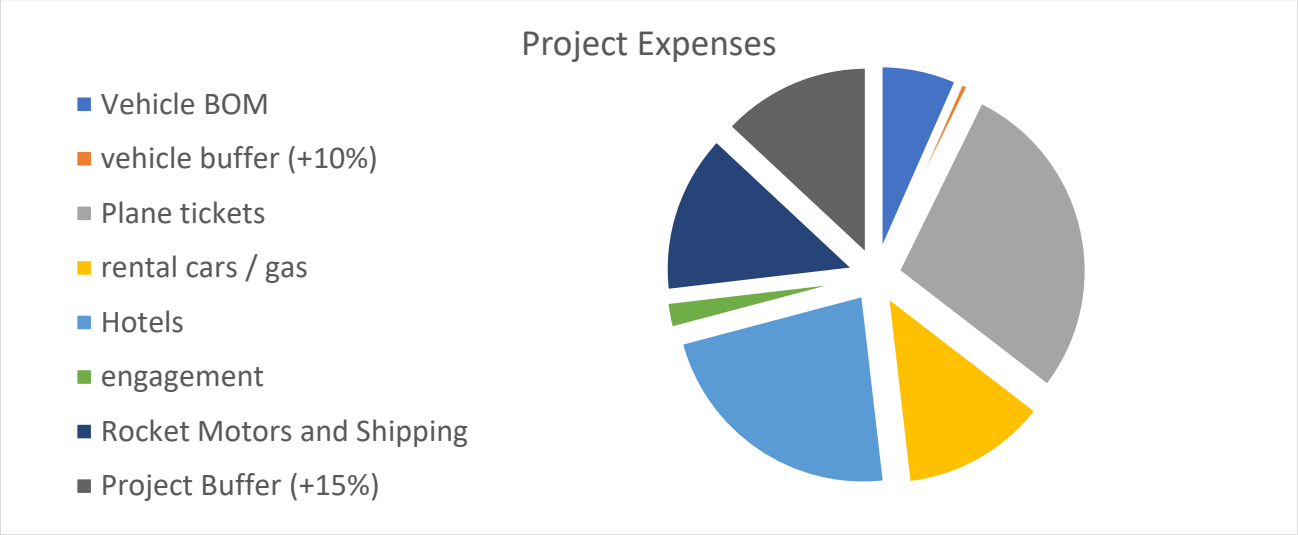

Figure 6.2.1: Pie-Chart of Expected Expenses

Travel Expenses (plane tickets, hotels) are based on the cost of 10 members traveling to Huntsville, AL. for 6 days and 5 nights. Rental car/gas cost is based on getting 3 cars in Hurstville and paying for gas for members driving to test launches during the full-scale vehicle test period.

6.2.3 Funding Plan

The Funding plan remains largely unchanged since the proposal, with 5 main sources of funding coming into our club: Student Government Association, The College of Engineering Deans Office, The Department of Mechanical and Industrial Engineering, GiveCampus crowdsourcing campaign, and corporate sponsorships.

6.2.3.1 Student Government Association

The team received $1324 from the Student Government Association for the annual budget and the business team is currently working on a grant request that can supply an additional $1800 to the club.

6.2.3.2 Francis College of Engineering Deans Office

We received the full amount of $2500 from the FCOE Deans Office, largely in part to our continued assistance with club fairs, open houses, and other events around campus.

6.2.3.3 Department of Mechanical and Industrial Engineering (MIE)

The business team will arrange a meeting with the Chair of the MIE department before the end of the semester to request additional funding from the department.

6.2.3.4 GiveCampus Crowdsource Fundraising

The business team is currently editing a promotional video for a GiveCapmus page, a GoFundMe style website for college groups to raise money. The goal is to get the campaign started before the holiday season so members can share the link amongst their families.

6.2.3.5 Corporate Sponsorships

Lastly the business team has reached out to Kerry Pucillo, who manages corporate relations at UML. The team will soon start reaching out to local businesses and engineering firms to see if they are interested in sponsoring the team.

6.3 Project Timeline – Gantt Chart

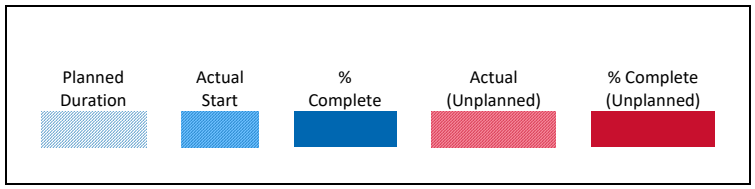

Figure 6.3.1: Project Timeline Legend

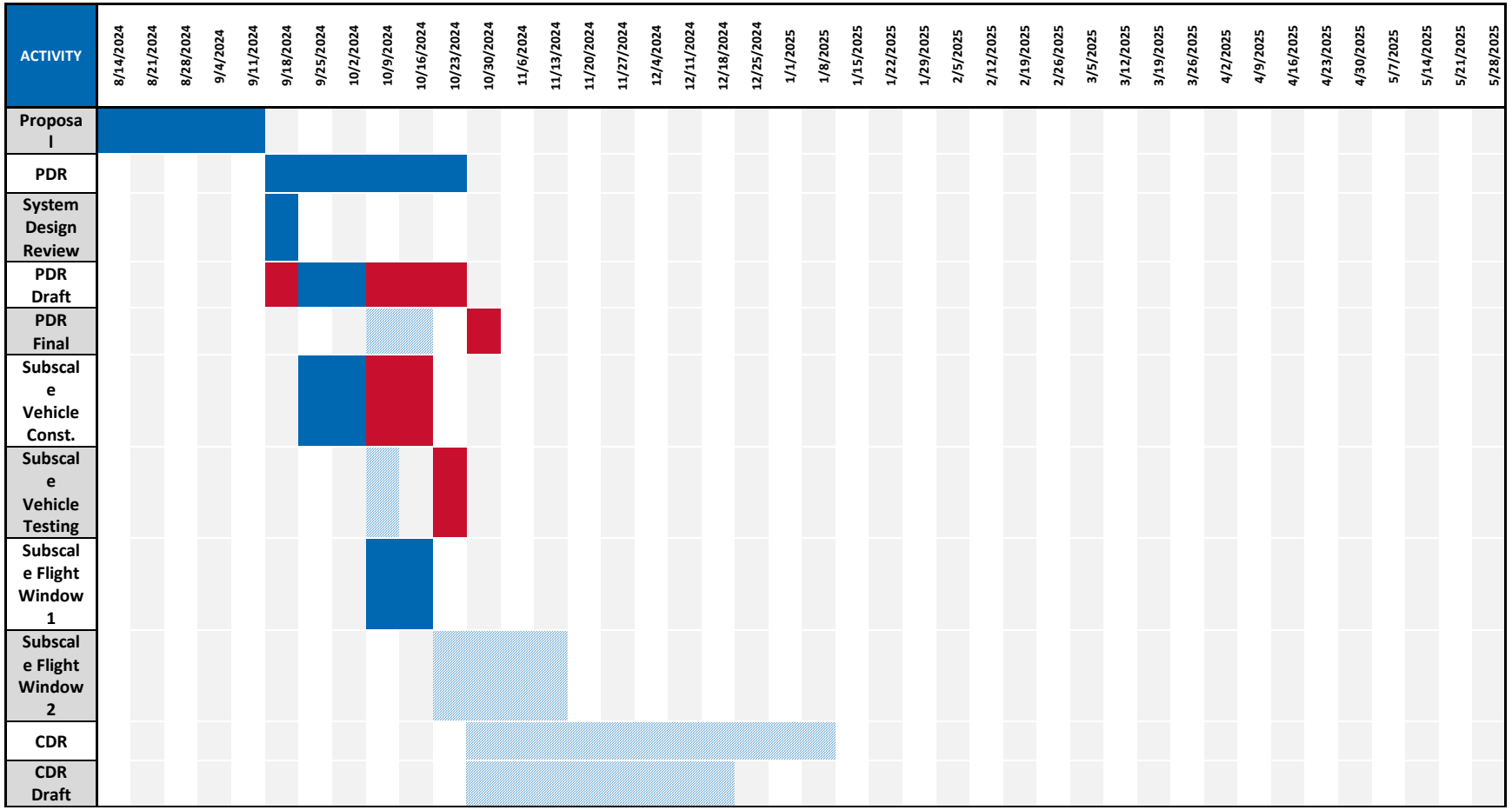

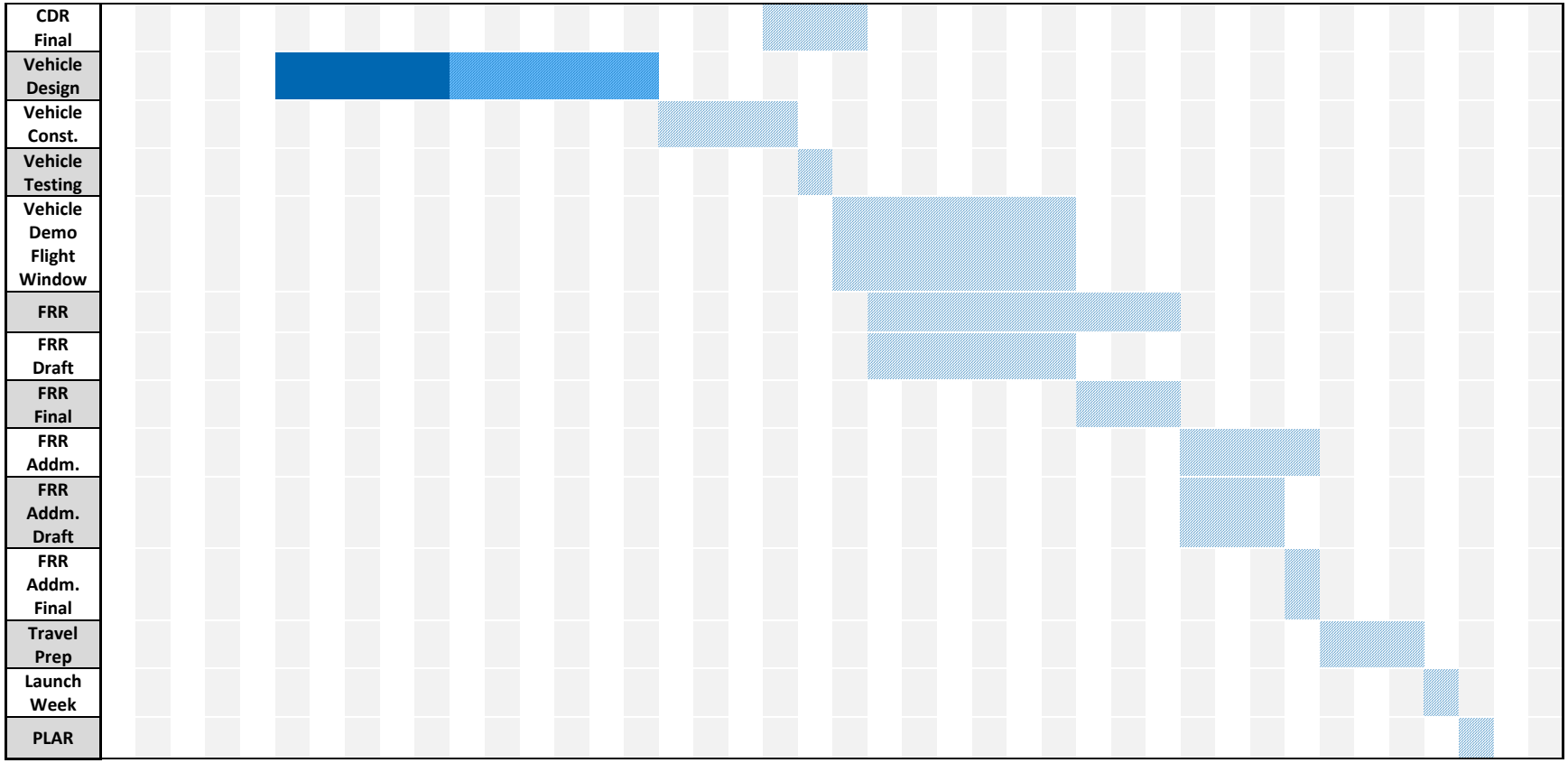

Figure 6.3.2: Project Timeline